Article

A Genetic Model for the Biggenden Gold-Bearing Fe Skarn Deposit, Queensland, Australia: Geology, Mineralogy, Isotope Geochemistry, and Fluid Inclusion Studies

Mansour Edraki [1], Alireza K. Somarin [2,*] and Paul M. Ashley [3]

[1] Sustainable Minerals Institute, The University of Queensland, St Lucia, QLD 4072, Australia; m.edraki@uq.edu.au
[2] Department of Geology, Brandon University, Brandon, MB R7A 6A9, Canada
[3] Earth Sciences, University of New England, Armidale, NSW 2351, Australia; papags47@gmail.com
[*] Correspondence: somarina@brandonu.ca

Abstract: The Biggenden gold-bearing Fe skarn deposit in southeast Queensland, Australia, is a calcic magnetite skarn that has been mined for Fe and gold (from the upper portion of the deposit). Skarn has replaced volcanic and sedimentary rocks of the Early Permian Gympie Group, which formed in different tectonic settings, including island arc, back arc, and mid-ocean ridge. This group has experienced a hornblende-hornfels grade of contact metamorphism due to the intrusion of the Late Triassic Degilbo Granite. The intrusion is a mildly oxidized I-type monzogranite that has geochemical characteristics intermediate between those of granitoids typically associated with Fe-Cu-Au and Sn-W-Mo skarn deposits. The skarn mineralogy indicates that there was an evolution from prograde to various retrograde assemblages. Prograde garnet ($Adr_{11-99}Grs_{1-78}Alm_{0-8}Sps_{0-11}$), clinopyroxene ($Di_{30-92}Hd_{7-65}Jo_{0-9}$), magnetite, and scapolite formed initially. Epidote and Cl-bearing amphibole (mainly ferropargasite) were the early retrograde minerals, followed by chlorite, calcite, actinolite, quartz, and sulfides. Late-stage retrograde reactions are indicated by the development of nontronite, calcite, and quartz. Gold is mainly associated with sulfide minerals in the retrograde sulfide stage. The fluids in equilibrium with the ore-stage calcites had $\delta^{13}C$ and $\delta^{18}O$ values that indicate deposition from magmatically derived fluids. The calculated $\delta^{18}O$ values of the fluids in equilibrium with the skarn magnetite also suggest a magmatic origin. However, the fluids in equilibrium with epidote were a mixture of magmatic and meteoric water, and the fluids that deposited chlorite were at least partly meteoric. δD values for the retrograde amphibole and epidote fall within the common range for magmatic water. Late-stage chlorite was deposited from metasomatic fluids depleted in deuterium (D), implying a meteoric water origin. Sulfur isotopic compositions of the Biggenden sulfides are similar to other skarn deposits worldwide and indicate that sulfur was most probably derived from a magmatic source. Based on the strontium ($^{87}Sr/^{86}Sr$) and lead ($^{206}Pb/^{204}Pb$, $^{207}Pb/^{204}Pb$ and $^{208}Pb/^{204}Pb$) isotope ratios, the volcanic and sedimentary rocks of the Gympie Group may have contributed part of the metals to the hydrothermal fluids. Lead isotope data are also consistent with a close age relationship between the mineralization at Biggenden and the crystallization of the Degilbo Granite. Microthermometric analysis indicates that there is an overall decrease in fluid temperature and salinity from the prograde skarn to retrograde alterations. Fluid inclusions in prograde skarn calcite and garnet yield homogenization temperatures of 500 to 600 °C and have salinities up to 45 equivalent wt % NaCl. Fluid inclusions in quartz and calcite from the retrograde sulfide-stage homogenized between 280 and 360 °C and have lower salinities (5–15 equivalent wt % NaCl). In a favored genetic model, hydrothermal fluids originated from the Degilbo Granite at depth and migrated through the shear zone,

intrusive contact, and permeable Gympie Group rocks and leached extra Fe and Ca and deposited magnetite upon reaction with the adjacent marble and basalt.

1. Introduction

The Biggenden mine in southeast Queensland, Australia (Figure 1) can be classified as an iron skarn, however, it has geochemical and mineralogical characteristics that overlap with worldwide gold and copper skarn deposits (e.g., [1–6]). There are also differences between the Biggenden deposit and other skarn deposits in terms of hydrothermal alteration and geochemical features of the adjacent pluton, Degilbo Granite.

The Biggenden mine was opened in 1888, and it was first operated for Cu, Au, and Bi. Quantities of commodities extracted from the mine are not accurately known, but approximate values provide some indication of the changing focus of mining. Early production of approximately 6000 ounces of gold (1888–1901) was followed by 200 tons of bismuth (1901–1938), with Commercial Minerals commencing open pit mining of magnetite in 1967. An estimated 580,000 tons of magnetite were produced for the Australian coal industry by 1990, during a transition into underground mining. The total measured recoverable reserve at Biggenden was estimated to be 107,000 tons of wet product, from 323,000 tons of ore with an average head grade of 30.7% magnetite [7]. The mine was closed in 1999 due to the exhaustion of economic resources.

The Biggenden skarn has been mentioned in review articles of world skarns [8,9] but has never been described in detail. Despite previous works (e.g., [10–12]), its genesis has long remained an enigma. The spectacular skarn exposures at the Biggenden mine resulting from three decades of open pit and underground mining offer an opportunity to study this deposit more closely and to apply new techniques to investigate the genesis of this deposit.
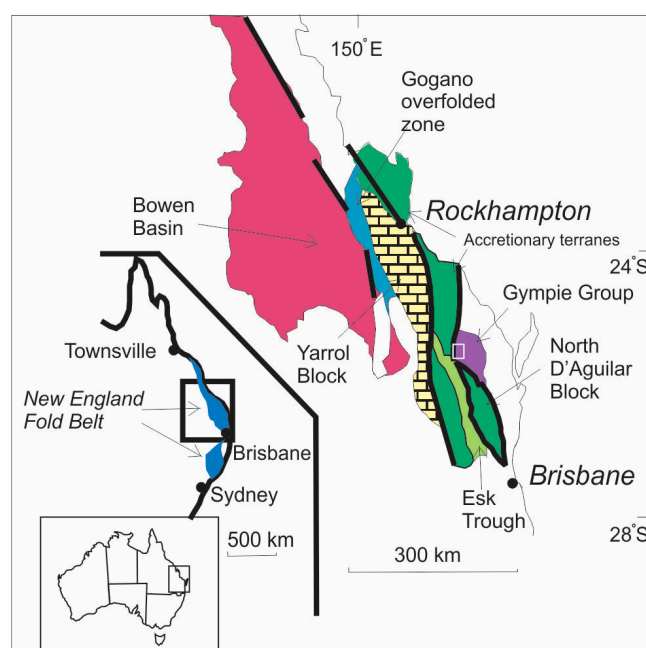
Figure 1. Major tectonic terranes of the Northern New England Orogen and the location of the Biggenden mine in the Gympie Group (also called Gympie Terrane [13]). Location of Figure 2 is shown as white rectangle. Modified after [14].

2. Regional Geological Setting

The Biggenden mine is situated in the Gympie Group, which is part of the New England Orogen, eastern Australia (Figure 1). Various origins have been suggested for the Gympie Group, ranging from an accreted arc to an exotic displaced terrane derived perhaps from New Zealand or New Caledonia [15–17] or, alternatively, that it represents a foreland basin originating not far from the Australian continental crust [13,18]. The mine area is underlain by the Early Permian rocks of the Gympie Group in the east and the Late Triassic Degilbo Granite in the west (Figure 2). The Gympie Group sequence is steeply dipping and locally faulted, sheared, and folded, and affected by the lowermost greenschist facies metamorphism. To the south, the Triassic Mount Marcella Volcanics overlie the Gympie Group, and in some places, Pleistocene Barambah Basalt overlies all the units, especially [15]. The host rocks for mineralization at the Biggenden mine area comprise intercalated basaltic and andesitic flows, tuffaceous and fragmental rocks of sedimentary/volcanic provenance, siltstone, and limestone (Figure 3). The basalts are partly vesicular with local pillow structures. Dolerite dikes also occur to the northeast of the Biggenden mine. Geochemical studies of the volcanic rocks of the Gympie Group suggest that these rocks formed in different tectonic settings, including island arc, back arc, and mid-ocean ridge settings [17,19,20], and were tectonically juxtaposed in the Triassic.
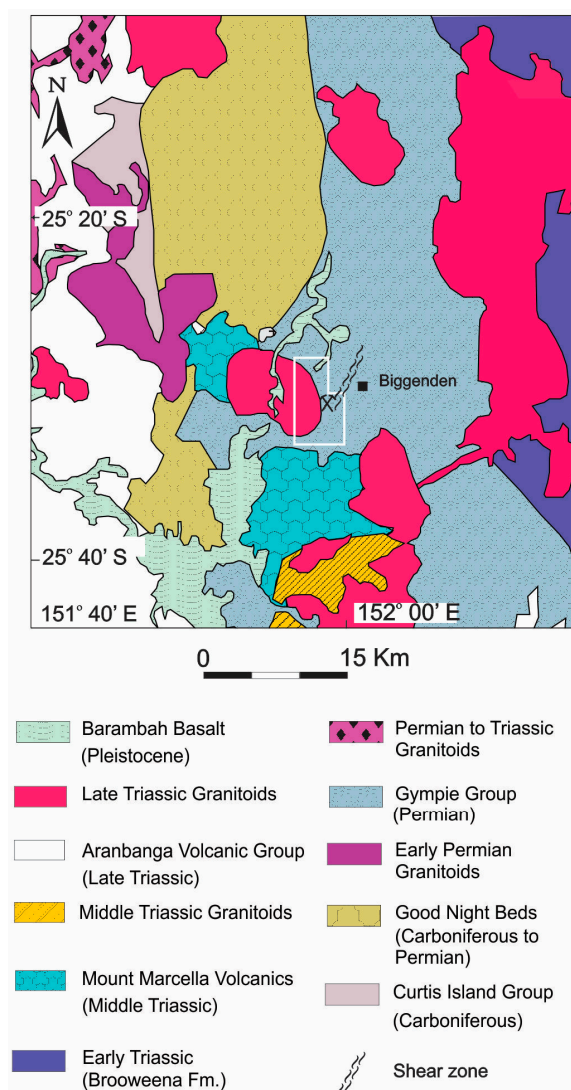
Figure 2. Regional geological map of the Biggenden mine area. Location of Figure 3 is shown as white rectangle. Geology modified after [15].
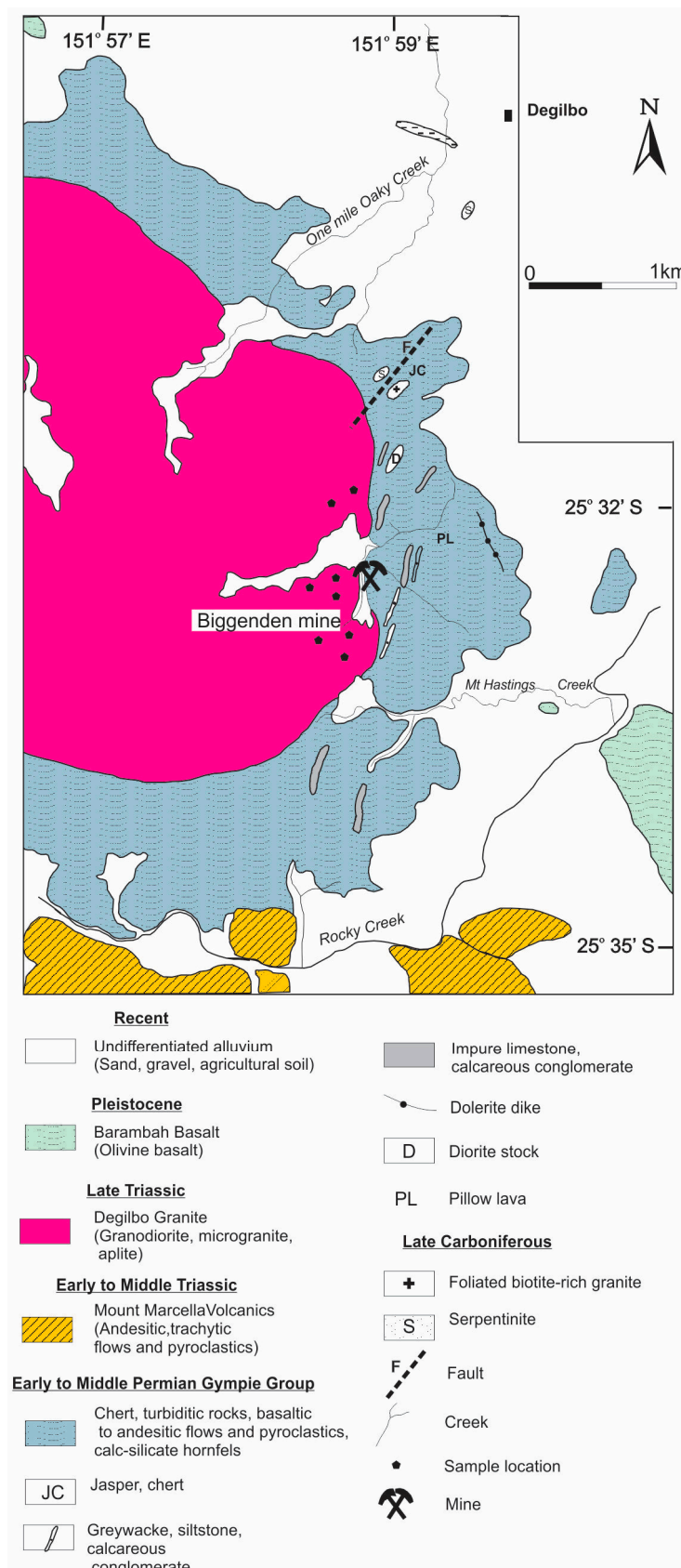
Figure 3. Geological map of the open pit area at the Biggenden mine (after [15]).

The Degilbo Granite is a massive, biotite-hornblende monzogranite of I-type affinity, and except for evidence of minor actinolite endoskarn vein development at the Biggenden mine, it is generally unaltered. It has intruded and is in most parts surrounded by the

Gympie Group, except in the western contact, where it has intruded the andesitic flows and pyroclastics of the Mount Marcella Volcanics. The age of the pluton has been reported to be 220 Ma (a K-Ar biotite age [21]) and 216 ± 6 Ma (a K-Ar age on contact metamorphic hornblende [15]).

Other prospects and abandoned mines in the area are aligned roughly north-south with the Biggenden deposit and are mainly concentrated along the eastern margin of the Degilbo Granite (Figure 3). To the north of the area, in the vicinity of the Commonwealth mine (Figure 3), there are outcrops of small masses of serpentinite and foliated biotite granite that are associated with an NE-trending fault. This biotite granite is distinguished from the Degilbo Granite based on its mineralogy, texture, and deformation. The biotite granite is interpreted to be older and part of a fault melange [19].

Mine Geology

The Gympie Group in the mine area (~2 km^2) consists of five primary rock units:

1. Lava Flows: These amygdaloidal basalts and andesites occur in the eastern part of the open pit and display coherent volcanic flow textures. They feature intergranular, subophitic, or porphyritic textures, with albitized plagioclase laths and augite in a groundmass of altered plagioclase, ferromagnesian minerals, and accessory titanomagnetite and ilmenite. The amygdales, up to 1 cm, are filled mainly with epidote and chlorite.

2. Volcaniclastic Rocks: These rocks are closely associated with the lava flows but differ in their dominant fragmental texture. The outcrops in the open pit transition from a gradational contact with the volcanic flows to a gradational contact with polymictic rocks.

3. Polymictic Rocks: This unit, found between the granite contact and the volcaniclastic unit, includes a tuffaceous lithic wacke and breccia. These rocks are black to greenish-black, due to the presence of metamorphic hornblende, clinopyroxene, and biotite. The key difference from the volcaniclastic unit is the inclusion of non-volcanic clasts such as chert, siltstone, and limestone. Contact metamorphism has replaced some of these fragments with calc-silicate minerals.

4. Limestone: The mine area features several large and small marble bodies, with a granoblastic polygonal texture. Over 98% of the rock is calcite, with disseminated garnet and other common calc-silicate minerals.

5. Metasiltstone: This unit is an orange-brown, intensely jointed horizon in the open pit area. It has a granoblastic texture and locally contains up to 50% metamorphic biotite near the contact zone.

The Degilbo Granite is medium to coarse-grained with a hypidiomorphic granular texture and is locally porphyritic, containing phenocrysts of pink perthitic K-feldspar and white plagioclase. There is no significant mineralogical variation within the granite, and no notable endoskarn has developed. A few aplite and microgranite porphyry dikes cut through the granite and surrounding rocks, suggesting late-stage offshoots of the main granite body. The pink color of the K-feldspar and characteristic minerals, including hornblende, titanite, allanite, and magnetite, are typical of I-type granites [22,23].

The orebody at Biggenden formed through metasomatic replacement (exoskarn) of various protoliths in the Gympie Group. The orebody is 360 m long, up to 35 m wide, and extends to a depth of approximately 135 m. Magnetite occurs in large, irregular masses, lenses, veins, and disseminated grains. The strata strike N-S to N10° E and dip steeply west, possibly indicating subvertical thrust stacks [15]. A near-vertical shear zone occurs close to the granite contact, extending up to 30 m away. Stronger mineralization is found near shear zones. Contact metamorphic minerals overprint the shear fabric, with mineralization

observed in pressure shadow tails and boudinage structures. Aeromagnetic data [24] reveal a northeast-striking linear structure, approximately 5 km long and 200 m wide, which includes the shear zone at the mine. Previous studies by Cranfield (1994) [15] also report a regional shear zone extending northeast of the Biggenden mine.

The prominent hanging wall fault, striking parallel to the western margin of the magnetite orebody (Figure 4A), is barren and filled with clay gouge. The most recent movement on this fault post-dates mineralization and is likely post-granite emplacement, as the gouge is not metamorphosed. Broad zones of brecciation, up to several meters wide, occur in the mine, particularly in association with marble (Figure 4B). Breccia fragments, up to 0.5 m in size, are composed of hornfels, mainly formed from polymictic rocks, which are replaced at the margins by garnet and magnetite. No significant structural displacements of the orebody have been observed that could explain its proximity to the unaltered granite (Figure 5).
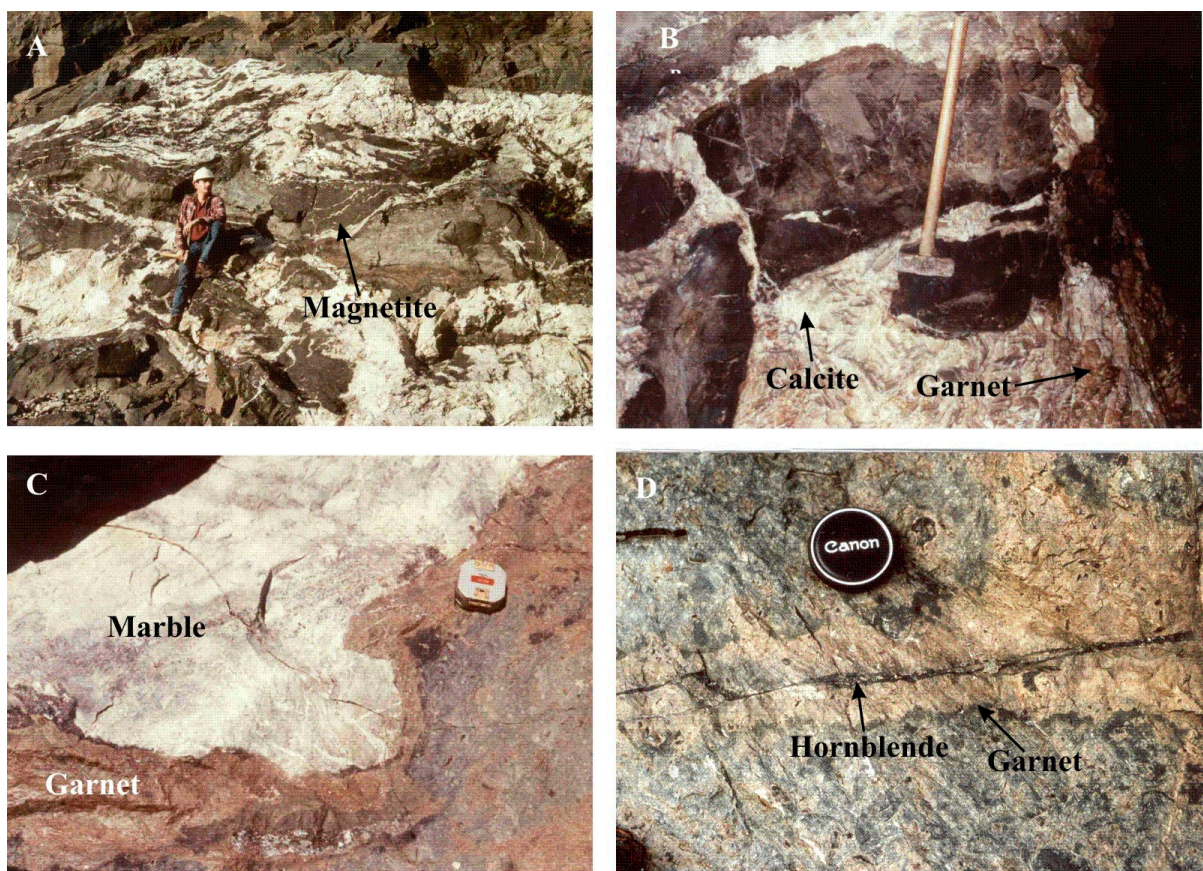
Figure 4. Photographs showing field features at the Biggenden mine. (**A**) Part of the open pit shows outcrops of dark-brown-gray lenticular magnetite bodies set in a cement of coarse-grained hydrothermal calcite. Lenses of marble occur behind and to the right of the person in the photograph. The upper part of the photograph shows outcrops of hornfels. (**B**) Brecciation showing meter-size fragments of breccia set in a cement of coarse calcite. Fragments comprise magnetite, skarn silicates (predominantly garnet), and remnants of the hornfels protoliths. (**C**) Garnet assemblage formed as reaction skarn at the contact of marble and volcaniclastic rocks. (**D**) Prograde veining and replacement of the volcaniclastic rocks at the open pit by garnet skarn are followed by the deposition of hornblende at a later retrograde stage.
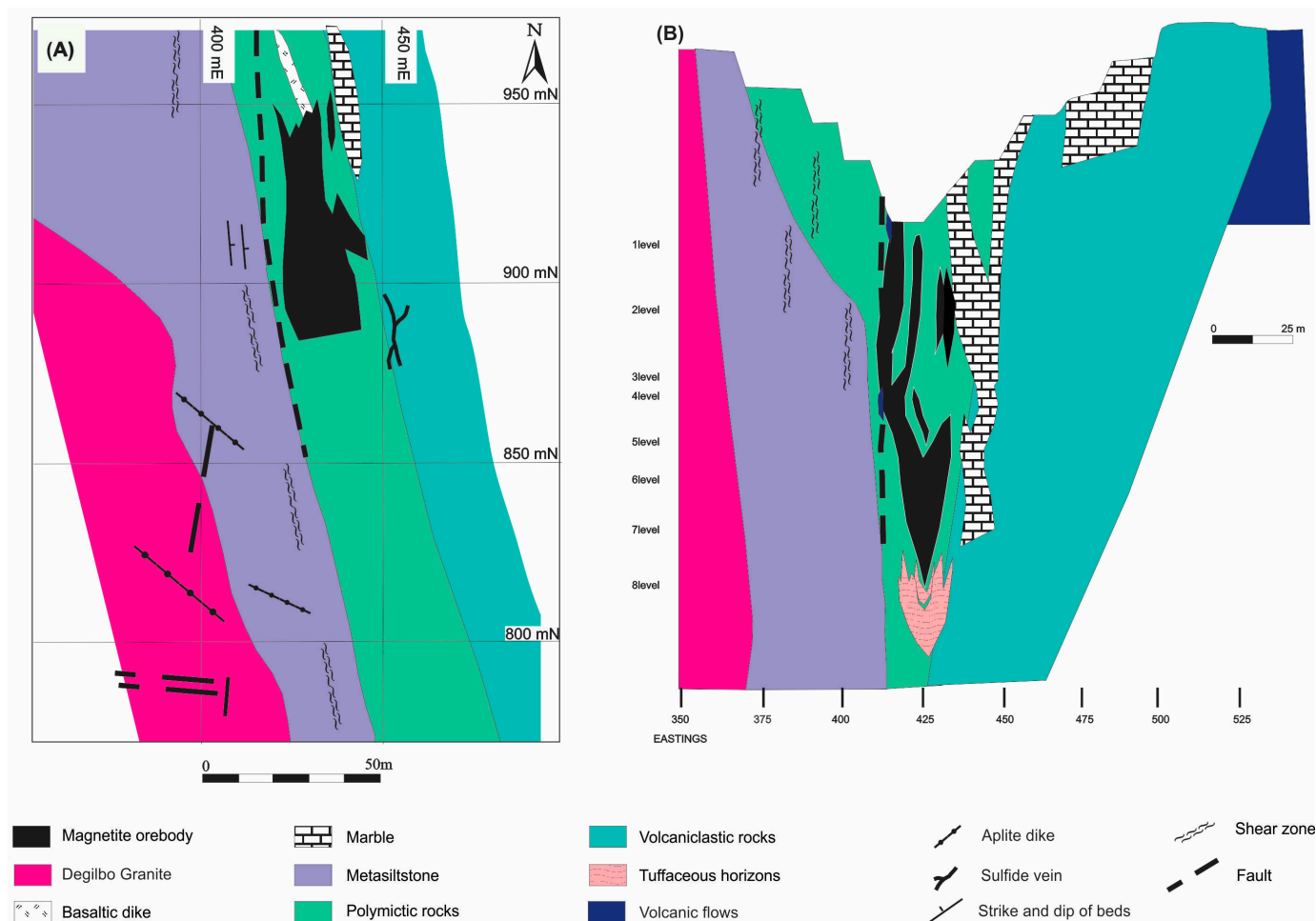
Figure 5. Geology of level 5 at the Biggenden mine (**A**) and cross-section along line 950 mN (**B**) (after [7]; Edraki, 2000 [15]).

3. Materials and Methods

The geochemistry of the intrusive rocks has been investigated in 19 samples, including Degilbo Granite, microgranite, and aplite dikes. Samples were analyzed by XRF at the University of New England (UNE) for major and trace elements. Microanalysis of metamorphic and skarn minerals was carried out at University of New England, Armidale, Australia using a JEOL JSM 5800LV scanning electron microscope equipped with energy dispersive spectrometer (EDS). The acceleration potential, beam current, and analysis time were 20 kv, 20 μA, and 120 s, respectively.

Fluid inclusion samples were mainly collected from the ore and chlorite assemblages. Thermometric analyses were carried out on an SGE heating/freezing stage. Vapor-liquid homogenization temperature (T_h), last ice melting (T_m), and the disappearance temperature of salt (T_d) were recorded. Heating was carried out twice for each fluid inclusion, and an average was recorded as the homogenization temperature. The precision of the temperature measurements was ± 5 °C. The coexistence of vapor-rich and liquid-rich fluid inclusions in the same analyzed grains is considered to be representative of the boiling of hydrothermal fluid [25], and therefore pressure correction was not applied to the acquired homogenization temperatures.

All mineral separations and sample preparations for isotope analyses of carbonates and sulfides were performed at UNE. Sample preparations for silicates and all stable isotope analyses were carried out at the Centre for Isotope Studies at CSIRO, North Ryde, Australia. For oxygen isotope analysis, oxygen in the silicates and magnetite was extracted by the

BrF$_5$ technique according to the method of Clayton and Mayeda (1963) [26]. For hydrogen isotope analyses, water was extracted from the hydrous silicates according to the method of Friedman (1953) [27].

δ^{34}S values of the sulfides were determined on SO$_2$ gas, which was extracted from sulfide minerals by combustion with Cu$_2$O powder at 1100 $^\circ$C, according to the method of Robinson and Kusakabe (1975) [28]. Carbonates were prepared following the method of McCrea (1950) [29]. The values are reported here in the usual delta notation (δ) in per mil (‰) with δ^{13}C relative to V-PDB and δ^{18}O and δD relative to the V-SMOW standard.

For Sr isotope analysis, pulverized granite and other silicate rock samples were dissolved overnight in a Teflon bomb using HF, HNO$_3$, and HClO$_4$ at 180 $^\circ$C until digestion was complete. Carbonates were dissolved in CH$_3$COOH and HCl. Separation of Sr was conducted using standard cation exchange chromatography. The dissolved samples were centrifuged in 1 mL of 6 M HCl and then loaded on columns of ion-exchange resin. The separated Sr was loaded on W filaments and analyzed by thermal ionization mass spectrometry.

An accelerator mass spectrometer system called AUSTRALIS [30] was used for lead isotope analysis at CSIRO. The system enables in situ microanalysis of samples, and Pb isotope measurements were performed using a 30-micron microbeam in polished thin sections containing galena.

4. Results and Analysis

4.1. Mineralogy and Mineral Compositions

Major minerals in the Degilbo Granite include quartz, plagioclase, K-feldspar, hornblende, and biotite with accessory apatite, zircon, titanite, allanite, and magnetite. The intrusion of this granite has produced a hornblende hornfels grade of contact metamorphism in the rock units of the Gympie Group, extending up to 1.3 km from the intrusive contact. The lowest grade of contact metamorphism is represented by chlorite, epidote, albite, pale-green actinolite, quartz, and calcite in the mafic rocks consistent with the albite-epidote hornfels facies. As the pluton is approached, at approximately 700 m from the contact, green hornblende appears in the basalts and dolerites, and actinolite is partially replaced by hornblende. The highest-grade contact metamorphic rocks occur in the inner part of the aureole at a distance of up to 150 m from the granite contact. Hornblende generally increases in abundance, and biotite appears in association with hornblende. At the mine, garnet $\pm$ clinopyroxene-amphibole bands (reaction skarn) have formed at the contact of hornfels with blocks of marble (Figure 4C).

Skarn mineralogy indicates that there was an evolution from prograde through to various retrograde assemblages (Figure 6), as hydrous retrograde minerals overprinted anhydrous prograde assemblages (Figure 4D). The orebody has been formed by metasomatic replacement of several protolith types, however, no significant endoskarn was developed in the granite. The complex nature of the fluid pathways in the host rocks, diverse protoliths, and contrast in permeability among host rocks prevented the development of clear mineralogical zonation patterns such as those documented in other skarn deposits [3,8]. However, close to the granite contact, clinopyroxene and clinopyroxene-plagioclase-titanite $\pm$ scapolite are the dominant high-temperature prograde skarn assemblages. They form veins and lenses, predominantly in the polymictic rocks. Clinopyroxene is paragenetically the earliest mineral, and it is found as inclusions in other prograde skarn minerals, commonly garnet.

|	Prograde skarn	Retrograde alteration	Weathering derived oxidation minerals
Titanite	▬		
Clinopyroxene	▬		
Garnet	▬		
Scapolite	▬		
Plagioclase	▬ ▬	▬	
Amphibole	····	▬	
Epidote		▬	
Chlorite		▬	
Quartz	····	▬	
Calcite	▬	▬ ▬	
Clay minerals		▬	
Gold		▬	
Magnetite	▬	▬	
Hematite		▬ ▪ ▪	▪ ▪ ▪
Arsenopyrite		▬	
Bismuthinite		▬	
Cobaltite		▬	
Molybdenite		? ▬	
Pyrite		▬	
Tetrahedrite		▬	
Chalcopyrite		▬	
Sphalerite		▬	
Covellite			▬
Malachite			▬
Goethite			▬

Figure 6. Schematic diagram showing paragenetic stages of skarn formation and mineralization at the Biggenden mine. Short dash lines show discontinuous mineralization. Question mark indicates possible mineralization.

Garnet, magnetite, and calcite were mainly deposited within and close to the ore-body, where three prograde mineral assemblages are dominant: (1) garnet, (2) garnet-clinopyroxene, and (3) magnetite-garnet-calcite ± scapolite ± clinopyroxene. Scapolite replaces garnet and earlier-formed plagioclase; veinlets of scapolite commonly cut garnet and magnetite. Calcite was partially contemporaneous with magnetite and garnet based on textural evidence. Large euhedral crystals of calcite, up to a few centimeters in size, fill the fractures and matrix in the ore breccia. Late-stage calcite occurs as open-space-filling transparent crystals, up to a few cm in size, associated with clay and quartz.

The main retrograde assemblages include (1) amphibole, (2) amphibole-chlorite, (3) epidote-fibrous amphibole-calcite, (4) epidote-chlorite, (5) chlorite-quartz ± muscovite, with quartz, calcite, sulfides, and minor amounts of hematite, muscovite, apatite, and albite, and (6) montmorillonite-nontronite-calcite. Retrograde assemblages, particularly epidote-chlorite, are more abundant to the east of the ore zone, where the permeability of pyroclastic rocks may have controlled the distribution of these hydrous minerals.

Sulfides occur as disseminated grains, veins, and fracture fillings and are commonly associated with the retrograde assemblages (Figure 6). The average total sulfide content in the orebody is approximately 3 volume% with pyrite, chalcopyrite, and bismuthinite as the most common phases. Molybdenite, arsenopyrite, tetrahedrite, and trace cobaltite are also found locally as disseminated grains. Gold is dispersed erratically in trace amounts

through the orebody. It is mainly associated with bismuthinite and trace native bismuth (Figure 7), and like other gold-bearing iron skarn deposits, its presence is related to the abundance of sulfide minerals [31]. In the past, gold was mined from the "actinolite rock", which is part of the retrograde skarn [10]. A late-stage retrograde clay assemblage locally replaced both the prograde and earlier retrograde skarn minerals and is characterized by the abundance of montmorillonite, nontronite (determined by XRD), and calcite. At shallow depths, supergene oxidation has produced hematite, covellite, malachite, and goethite from the skarn assemblage.
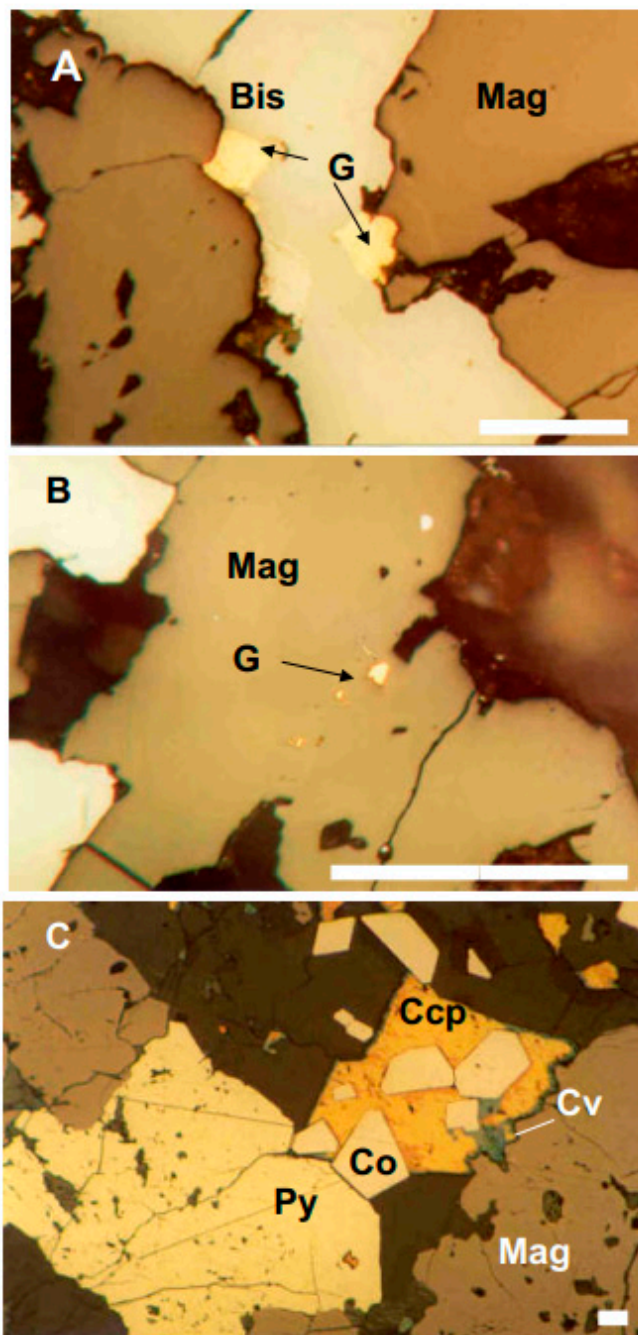
Figure 7. (**A**) Photomicrograph of gold (G) and bismuthinite (Bis) filling a fracture in magnetite (Mag) and/or replacing magnetite along a grain boundary. (**B**) Association of gold and magnetite. The linear arrangement of the small grains of gold may indicate that they follow a grain boundary in the magnetite aggregate. (**C**) Association of magnetite, pyrite (Py), chalcopyrite (Ccp), cobaltite (Co), and covellite (Cv). All are in reflected, plane-polarized light, and the scale bars are 50 μm.

Clinopyroxene is dominated by diopside-hedenbergite solid solution with minor johannsenite ($Di_{30-92}Hd_{7-65}Jo_{0-9}$) (Table 1). Pyroxene compositions fall within the fields of Fe and Au skarns (Figure 8). However, they are diopside-rich and are comparable to Cu skarns with respect to diopside content. The average Mn/Fe ratio for the Biggenden pyroxene is relatively high (0.12) for an iron skarn. Nakano et al. (1994) [32] have reported pyroxene with a high johannsenite component or Mn/Fe ratios in a few iron skarns in Japan. Matsueda (1981) [33] and Einaudi and Burt (1982) [34] also noted that some Fe skarns have high johannsenite-rich pyroxene. Gold skarn pyroxene can be more Al-rich than pyroxene in other skarn types [35]. The Al content of the Biggenden pyroxene is mainly comparable to Au skarns.

Scapolite is marialite-rich (average 76 mole% marialite) and Cl-bearing (Table 2). The proportions of marialite and Cl contents in Biggenden scapolite are similar to those in other gold and iron skarn deposits, e.g., Nickel Plate in British Columbia (Meionite 30–54 mole% and Cl = 1.7%–2.9% [36,37]).
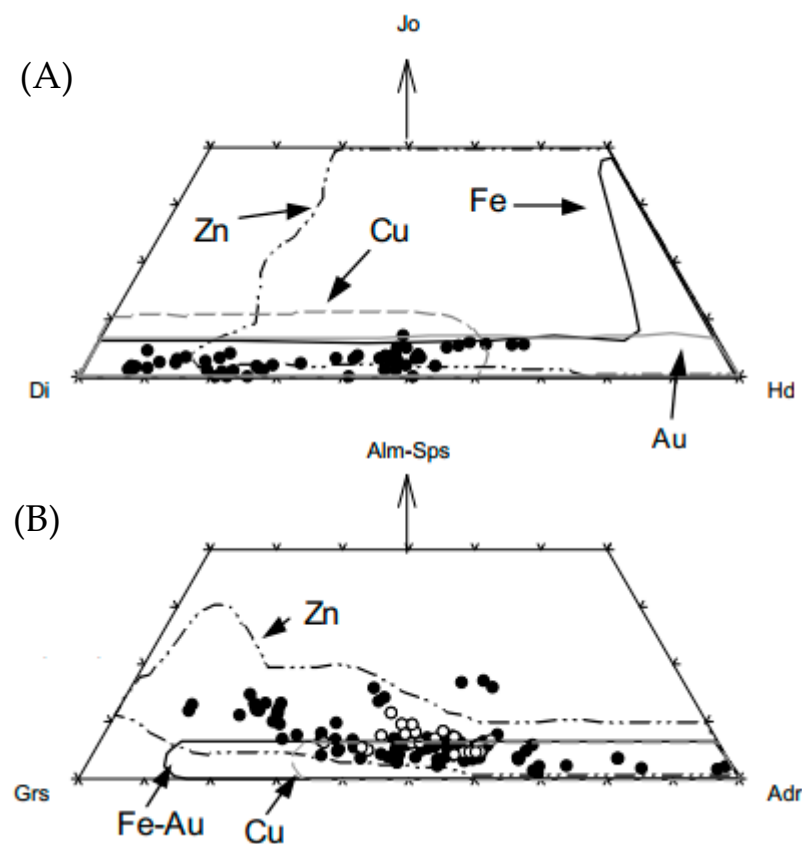
Figure 8. Ternary plots of Biggenden skarn clinopyroxene (**A**) and garnet (**B**) compositions (black circles) compared to Fe, Au, Zn, and Cu skarns [2]. The white circles represent garnets in the ore. Jo = Johannsenite, Hd = Hedenbergite, Di = Diopside, Alm-Sps = Almandine-spessartine, Adr = Andradite, Grs = Grossular.

The composition of plagioclase in the clinopyroxene-plagioclase assemblage is An_{95-99} mole%. Garnet grains are predominantly andradite-grossular solid solutions, containing commonly less than 10 mole% of other components and ranging in composition from Adr_{11} to Adr_{99} (Table 1). The earlier generation of garnet is isotropic and less commonly shows optical zonation. The later generation is anisotropic, grossular-rich, and forms overgrowth rims on isotropic garnets. The composition of Biggenden garnet is similar to the classical examples of iron skarns (Figure 8; e.g., those from western British Columbia [38]). However, the analyzed garnet grains are slightly enriched in Mn and may approach the compositions

of garnet in Zn skarns [1,2,32]. Magnetite in the Biggenden skarn is close to stoichiometric Fe_3O_4, with low Ti.

Table 1. Range of chemical composition of garnet, amphibole, epidote, chlorite, and scapolite from the Biggenden mine. The number of analyses is in parentheses.

	Garnet					Clinopyroxene		
Assemblage	Garnet-Pyroxene (2)	Magnetite Ore (2)	Garnet Skarn (2)	Calc-Silicate (2)		Garnet-Pyroxene (4)	Magnetite Ore (2)	Pyroxene-Plagioclase (4)
SiO_2	37.46–37.80	37.04–37.26	36.83–37.48	36.9–37.72	SiO_2	49.8–51.95	51.14–51.82	50.88–53.8
TiO_2	1.03–1.79	0.88–21.59	0.79–2.12	0.53–2.07	TiO_2	ND-0.43	ND-0.20	ND
Al_2O_3	8.64–9.23	9.40–11.15	5.93–8.77	9.86–11.73	Al_2O_3	1.22–1.85	1.50–2.87	0.20–0.92
Fe_2O_3 *	16.01–16.24	15.71–15.95	16.19–22.37	11.99–15.76	Fe_2O_3 *	0.85–1.92	ND-1.88	ND-1.30
FeO	0.32–0.72	0.89–2.04	0.28–0.65	1.01–6.79	FeO *	0.14–15.08	0.81–14.89	8.94–14.93
MnO	0.91–1.74	1.19–1.19	0.68–1.07	0.28–0.31	MnO	ND-1.31	1.47–1.55	0.35–1.32
MgO	ND	ND-0.96	ND-0.31	ND	MgO	9.68–14.84	8.49–16.18	9.18–13.08
CaO	32.72–33.6	30.8–33.15	32.79–33.29	29.21–33.69	CaO	22.97–25.77	22.60–24.26	21.84–23.84
Total	98.91–99.30	99.21–100.00	99.57–100	98.49–99.36	Total	99.15–100.91	99.49–100.17	99.39–100.09
	Number of ions on the basis of 24 O					Cations on the basis of 6 O		
Si	6.02–6.05	5.94–5.96	5.99–6.03	5.94–6.02	Si	1.87–1.99	1.90–1.97	1.96–2.01
Ti	0.12–0.22	0.11–0.19	0.1–0.26	0.06–0.25	Ti	ND-0.01	ND-0.01	ND
Al^{IV}	1.63–1.75	0.04–0.06	0.01–1.15	1.81–2.21	Al^{IV}	ND-0.07	0.03–0.10	ND-0.04
Al^{VI}	ND	1.71–2.06	ND-1.64	ND-0.06	Al^{VI}	ND-0.01	0.02–0.04	ND-0.01
Fe^{3+}	2.15–2.17	1.85–2.14	2.17–2.76	1.60–2.12	Fe^{3+}	0.03–0.19	ND-0.06	ND-0.04
Fe^{2+}	0.04–0.10	0.12–0.31	0.04–0.09	0.13–0.92	Fe^{2+}	0.03–0.48	0.03–0.48	0.28–0.49
Mn	0.12–0.24	0.16–0.31	0.1–0.15	0.04	Mn	ND-0.04	0.05	0.01–0.04
Mg	ND	ND-0.23	ND-0.08	ND	Mg	0.55–0.83	0.49–0.89	0.53–0.73
Ca	5.64–5.77	5.28–5.69	5.7–5.79	5.04–5.76	Ca	0.93–1.04	0.93–0.96	0.91–0.98
Total	16.01	16–16.01	16–16.03	16.00	Total	4.00	3.99–4.00	3.98–4.00
Pyrope	0.00	0.00–3.82	0.00–1.28	0.00	Johannsenite	0.0–4.5	4.5–5.0	1.1–3.9
Almandine	0.73–1.62	1.99–5.23	0.64–1.46	2.27–15.24	Diopside	51.4–77.8	47.9–87.3	50.1–71.5
Spessartine	2.08–3.97	2.70–2.71	1.59–2.44	0.64–0.70	Hedenbergite	20.5–47.4	8.2–47.1	27.4–45.9
Grossularite	36.75–37.19	36.79–39.14	24.69–34.93	29.35–50.34				
Andradite	57.23–60.44	49.11–58.51	61.17–71.8	46.76–54.71				

	Amphibole			Epidote (4)		Chlorite (5)		Scapolite
	Skarn (6)	Contact metamorphic (2)						
SiO_2	37.76–48.92	45.82–50.18	SiO_2	37.46–38.7	SiO_2	26.79–31.29	SiO_2	54.26–59.73
TiO_2	ND-0.50	ND	TiO_2	ND-0.27	Al_2O_3	16.5–18.79	Al_2O_3	25.09–26.34
Al_2O_3	4.68–15.17	7.42–12.89	Al_2O_3	22.54–24.7	FeO *	26.79–31.29	CaO	5.95–9.90
FeO	19.30–24.70	9.13–12.73	Fe_2O_3	10.44–3.32	MnO	0.75–1.170	Na_2O	7.56–8.92
MnO	0.71–1.03	ND-0.57	MnO	ND-0.33	MgO	6.75–15.01	K_2O	0.21–1.04
MgO	4.84–9.44	13.74–15.97	CaO	23.1–24.61	Total	86.48–89.24	Cl	ND-3.43
CaO	11.43–12.81	10.75–11.69	Na_2O	0.41–0.64			−O=Cl	ND-0.77
Na_2O	0.33–2.74	1.57–3.62	Total	96.34–98.87			Total	99.24–100.82
K_2O	0.28–1.87	0.22–0.26						
Cl	ND-0.72	ND-0.22						
−O=Cl	ND-0.16	ND-0.05						
Total	97.16–99.26	98.33–98.40						
	Number of ions on the basis of 23 O			Numbers of ions on the basis of 25 O				Number of ions on the basis of 25 O
Si	5.84–7.37	6.53–7.25	Si	5.98–6.11	Si	5.73–5.95	Si	7.58–8.31
Al^{IV}	0.63–2.16	0.75–1.47	Ti	ND-0.03	Al^{IV}	2.05–2.27	Al	4.12–4.34
Al^{VI}	0.20–0.65	0.52–0.69	Al	4.22–4.64	Al^{VI}	1.97–2.65	Ca	0.89–1.48
Ti	ND-0.06	ND	Fe^{3+}	1.25–1.59	Fe^{2+}	4.75–6.34	Na	2.06–2.41
Fe^{3+} *	0.05–0.48	0.12–0.36	Mn	ND-0.04	Mn	0.14–0.21	K	0.04–0.18
Fe^{2+}	1.97–3.09	0.56–1.41	Ca	3.93–4.18	Mg	2.44–4.74	Cl	ND-0.82
Mn	0.09–0.13	ND-0.07	Na	0.13–0.20			Total	15.65–16.45
Mg	1.12–2.12	2.96–3.39	Total	16.06–16.16	Total cations	19.24–19.71		
Ca	1.91–2.07	1.64–1.81						
Na	0.10–0.83	0.44–1.00	Clinozoisite	73.50–80.20				
K	0.05–0.37	0.04–0.05	Pistacite	19.80–26.50				
Cl	0.00–0.19	ND-0.05	Piemontite	0–0.80				
Total cations	15.17–16.12	15.44–15.68						

* Recalculated based on stoichiometry. ND = Not detected.

Table 2. Representative chemical analyses of the Degilbo Granite and related dikes. Oxides and trace elements are in weight% and ppm, respectively.

Sample	R76342	R76340	R76343	R76344	R76345	R76346	R76410	R76366	R76458	R76325	R76440	R76368	R76337
						Granite						Microgranite Dike	Aplite Dike
Distance from Contact	600 m	500 m	200 m	150 m	100 m	80 m	60 m	50 m	3 m	1 m	20 cm		
SiO$_2$	68.94	68.87	71.09	69.38	69.22	69.23	68.86	70.31	68.3	63.9	63.92	70.06	77.17
TiO$_2$	0.41	0.45	0.35	0.54	0.43	0.42	0.4	0.37	0.44	0.69	0.67	0.43	0.09
Al$_2$O$_3$	15.44	15.37	14.73	14.49	15.2	15.42	15.19	14.59	15.65	16.82	18.16	15.23	12.49
Fe$_2$O$_3$	1.49	1.19	1.12	1.34	1.30	1.34	1.30	1.13	1.16	1.42	1.25	0.08	0.35
FeO	1.43	1.77	1.41	2.12	1.72	1.66	1.57	1.55	1.72	2.85	2.20	1.78	0.25
MnO	0.06	0.07	0.05	0.07	0.06	0.05	0.05	0.07	0.06	0.11	0.09	0.04	0.03
MgO	0.79	0.95	0.66	1.03	0.85	0.79	0.89	0.79	0.86	1.31	1.25	0.77	0.11
CaO	2.14	2.03	1.74	1.93	2.06	2.00	1.94	1.69	2.33	3.15	3.12	2.24	0.63
Na$_2$O	3.66	3.63	3.56	3.52	3.73	3.70	3.76	3.66	3.83	4.13	4.92	3.72	3.39
K$_2$O	4.46	4.30	4.50	4.26	4.23	4.24	4.28	4.29	4.35	3.72	2.75	3.64	4.78
P$_2$O$_5$	0.15	0.15	0.11	0.17	0.14	0.15	0.13	0.13	0.15	0.24	0.09	0.13	0.01
S	0.01	0.02	0.01	0.01	0.01	0.01	0.01	0.01	0.01	0.01	0.02	0.14	0.02
LOI	0.73	0.94	0.58	0.74	0.67	0.71	0.77	0.77	0.74	1.00	1.05	0.85	0.56
Total	99.69	99.74	99.9	99.58	99.58	99.71	99.13	99.34	99.6	99.34	99.46	99.08	99.85
Ba	735	704	607	735	627	669	742	703	610	818	541	691	80
Rb	179	170	181	179	187	182	181	195	184	161	138	135	259
Sr	273	248	213	273	205	250	264	251	216	280	381	248	33
Pb	17	16	19	17	19	16	16	14	17	20	19	17	24
Th	17	20	33	17	22	18	15	18	23	16	21	58	62
U	3	4	4	3	4	4	2	3	5	4	4	6	17
Zr	240	249	218	240	304	246	233	239	215	244	541	211	87
Nb	10	10	13	10	13	10	10	9	11	8	16	12	9
Y	32	34	35	32	43	36	37	34	34	28	22	33	25
La	36	43	35	36	45	41	37	41	33	42	46	28	24
Ce	65	69	63	65	83	75	72	67	55	72	78	52	41
Nd	31	32	30	31	44	35	32	32	25	30	37	25	18
Sc	7	7	7	7	16	7	6	9	4	13	14	6	3
V	30	34	24	30	38	32	33	34	30	33	39	29	5
Cr	11	7	6	11	13	10	11	5	12	7	13	7	2
Ni	6	5	3	6	5	6	6	3	3	5	6	4	4
Cu	9	13	45	9	25	14	13	13	8	14	16	95	2
Zn	36	43	37	36	48	40	37	36	50	46	61	43	38
Ga	17	16	16	17	17	18	17	18	17	17	19	16	15
Sn	<3	<3	9	<3	8	4	<3	10	<3	<3	<3	<3	<3
As	5	4	4	5	4	5	4	6	11	6	9	352	58
Mo	2	11	2	2	1	<1	6	3	1	2	15	1	2
Bi	4	73	3	4	2	5	<1	<1	1	2	5	5	2

The Biggenden skarn amphibole belongs to the ferropargasite and hastingsite groups (Table 1) and shows a continuous variation from $Fe^{3+} < Al^{VI}$ to $Fe^{3+} > Al^{VI}$ with up to 1.29% Cl. These amphibole grains resemble those in both Au and Fe skarns with regard to Fe, Mg, Mn, Ca, Al, Na, and K contents [2]. Epidote ranges in composition from 19.8 to 29.3 mole% pistacite with low piemontite content (Table 1). Chlorite is dominantly chamosite with $\Sigma Fe/Fe + Mg$ ratio ranging from 0.50 to 0.72 (Table 1). The range of calculated temperature for the retrograde skarn, using the chlorite geothermometer of Cathelineau (1988) [39], is between 252 °C and 375 °C, with an average of 310 °C.

4.2. Geochemistry of the Degilbo Granite

Based on modal mineralogy and using the classification scheme of Le Bas and Streckeisen (1991) [40], the Degilbo Granite is a monzogranite in composition. The whole rock chemical analyses of samples from the Degilbo Granite show a restricted compositional range, and the variations among samples are not related to the distance from the margin of the pluton (Table 2, Figure 9). There is a range of SiO$_2$ content from 68 to 71%, except for samples R76325 and R76440 which may be affected by incipient actinolite endoskarn development and consequently have lower SiO$_2$ values. The granite contains high

K$_2$O, K/(K + Na), Rb, Pb, and Th and is a high-K granitoid according to the classification of Peccerillo and Taylor (1976) [41]. It is mildly peraluminous (0%–1.63% normative corundum), and the Alumina Saturation Indices (ASI = molar Al$_2$O$_3$/CaO + Na$_2$O + K$_2$O) in all analyzed samples are less than 1.1, which is considered to be typical in I-type granites [22].
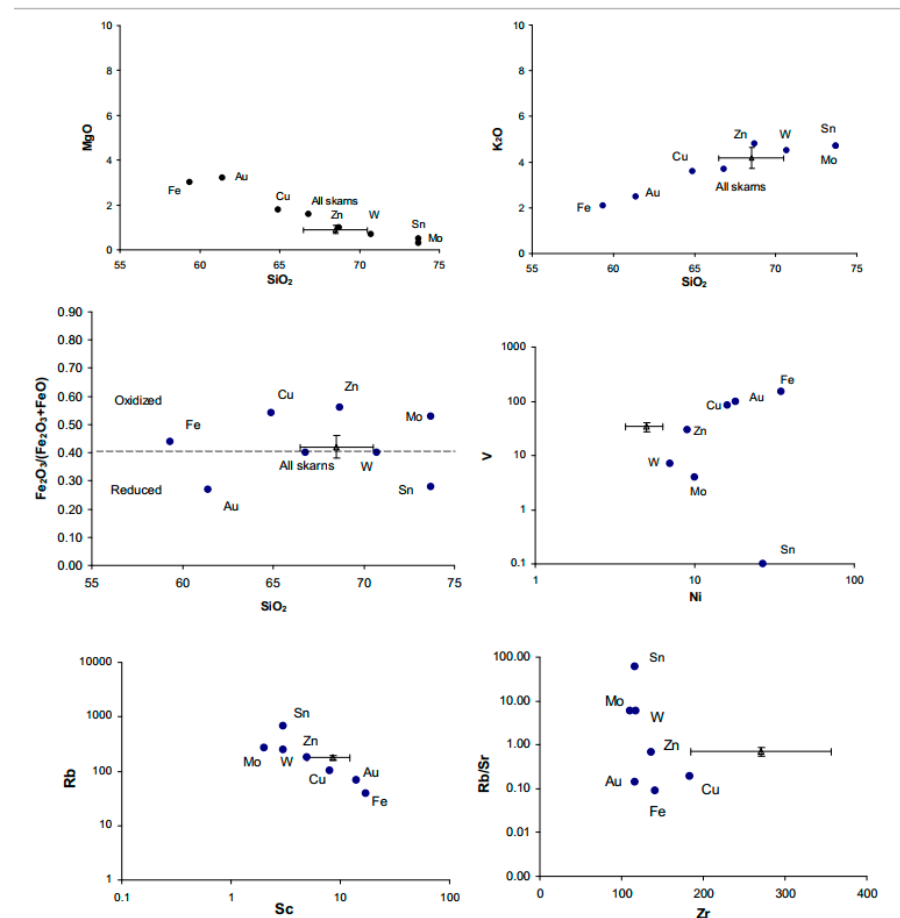
Figure 9. Average major and trace element content of plutons associated with different types of skarn deposits (filled circles after [3,8]), compared to the average composition of the Degilbo Granite (triangle, data from Table 2). Bars show the range of compositions of analyzed samples.

4.3. Microthermometric Studies

Fluid inclusions of measurable size (>5 microns) are present in garnet, quartz, and calcite from the Biggenden skarn assemblage. They are divided into three main types based on the major phases present. Type I fluid inclusions contain an aqueous liquid phase (L), a vapor phase (V), and one or several daughter crystals (S) and are commonly primary (using the criteria of Roedder, 1984 [26]). They are typically found in calcite grains in ore assemblages. Cubic, isotropic, and colorless crystals of halite are the main solid daughter phase in type I inclusions. The second isotropic daughter phase with a round shape was identified as sylvite based on its lower melting temperature. In some of the type I fluid inclusions, prismatic crystals, which are commonly smaller than halite, are also present. These daughter crystals did not change upon heating and are identified as anhydrites. Two types of opaque solid phases are present in these fluid inclusions; cubic grains possibly entrapped in magnetite and an unknown irregular solid phase attached to halite crystals.

Type II fluid inclusions are the most abundant and are characterized by a high proportion of liquid, with vapor content ranging from 10 to 40 volume% at room temperature. They are both primary and secondary or pseudosecondary, and the vapor homogenizes into a liquid phase upon heating.

Type III inclusions are less common and are characterized by a high proportion of gas ranging from 70 to 100 volume% and homogenize into a gas phase. Some of the inclusions of this type contain gas phase only, which may indicate that the fluids were trapped near the two-phase curve [26].

Fluid inclusions in calcite occur in various sizes and shapes and include all three types, with sizes ranging from less than 10 to 30 μm. Fluid inclusions in quartz are type II (V + L) inclusions, have irregular shapes, and range in size from 10 to 50 μm. Fluid inclusions in garnet are less abundant; they are two-phase (type II), have irregular shapes, and are commonly less than 10 μm in size, although in one sample, larger fluid inclusions up to 30 μm were found. Only a few measurements of T_h were obtained from fluid inclusions in garnet, as on heating above 500 °C the host mineral commonly became dark brown and fluid inclusions were obscured. The majority of analyzed fluid inclusions homogenized to a liquid phase. However, a few calcite samples contained scattered vapor-rich, type III inclusions that commonly homogenized into a vapor phase and are interpreted to reflect trapping under boiling conditions. The scarcity of this type of inclusion may imply that boiling occurred only locally or intermittently (cf. [42–44]).

4.3.1. Homogenization Temperatures

Two types of primary fluid inclusions are recognized based on homogenization temperature (Figure 10): (1) high-temperature (500–560 °C) fluid inclusions that are found in garnet and calcite from the magnetite ore assemblage, (2) moderate-temperature (280 °C to 360 °C) fluid inclusions in calcite and quartz from the retrograde (mainly chlorite) assemblage. A few inclusions in calcite (outside the ore assemblage) homogenize between 380 °C and 440 °C. Homogenization temperature in the secondary and pseudosecondary fluid inclusions ranges from 200 °C to 280 °C.
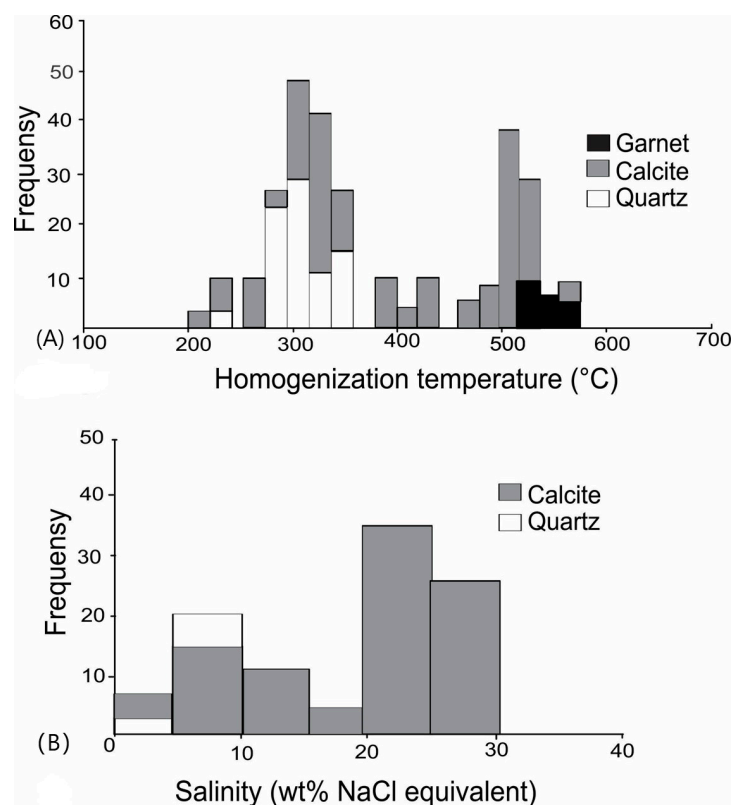

Figure 10. (**A**) Frequency distribution of the homogenization temperatures of primary fluid inclusions in garnet, calcite, and quartz samples. (**B**) Frequency distribution of the salinity (wt % equiv NaCl) based on the last ice melting and halite dissolution temperature measurements.

4.3.2. Salinities

Salinities of the fluid inclusions were measured from either the last ice melting temperature [45] or the halite dissolution temperature [46]. Halite in type I fluid inclusions was dissolved at temperatures between 240 °C and 386 °C, corresponding to 31 and 43 wt % NaCl equivalent. Type II (L + V) fluid inclusions show a bimodal distribution of salinity; one group between 5 and 15 wt % NaCl equivalent and the other group between 20 and 30 wt % NaCl equivalent (Figure 10). The latter is mainly from fluid inclusions with higher homogenization temperatures.

4.4. Isotope Geochemistry

$\delta^{18}O$ *and* $\delta^{13}C$ *in carbonates*: Samples of various generations of calcite, as well as marble, limestone, and calc-silicate hornfels, were analyzed for oxygen and carbon isotopes (Table 3). Skarn calcite, which occurs interstitially between skarn silicates and magnetite, has $\delta^{18}O$ values ranging from 9.6 to 12.2% and $\delta^{13}C$ values ranging from −0.7 to −7.1%. Average $\delta^{18}O$ and $\delta^{13}C$ in marble samples are 20.9% and 4.9%, respectively. Skarn calcite samples have oxygen and carbon isotope values only slightly different from those of fine-grained calcite samples (Figure 11). Although limestone has a eutectic melting temperature of 600–675 °C [47], evidence of limestone melting (e.g., melt inclusions; [48]) was not found in the Biggenden skarn. One calcite sample plot in the igneous field on the $\delta^{18}O$ and $\delta^{13}C$ diagram (Figure 11), which may be due to the intensive reaction of the limestone with magmatic fluid. Calcite formed in the latest stage of retrograde hydrothermal alteration has $\delta^{13}C$ values that reflect the skarn calcite compositions but have heavier $\delta^{18}O$ values, which are comparable to those of marine carbonates [49]. In marbles, despite recrystallization, the marine limestone isotopic signature has been retained. The carbon isotopic values for the calc-silicate hornfels are lower than those in the limestones (Table 3).
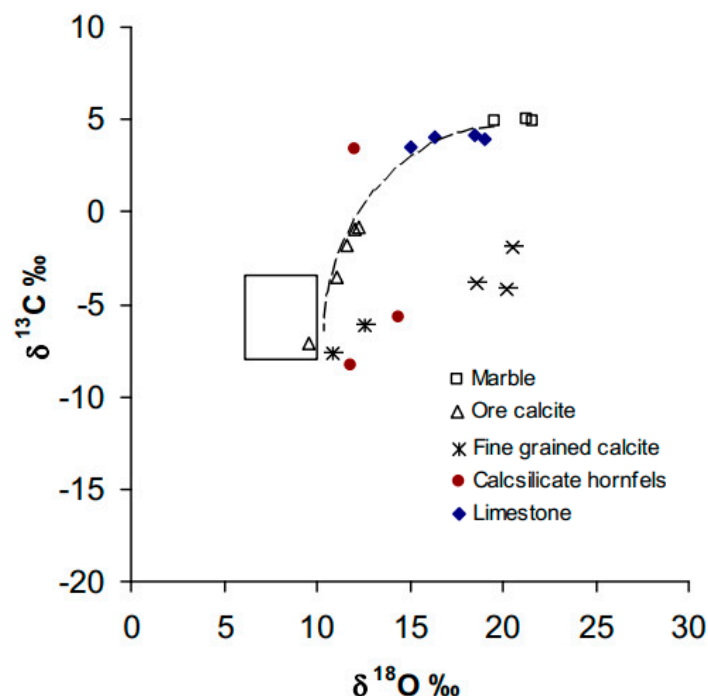
Figure 11. Carbon versus oxygen isotope diagram showing the isotopic compositions of the marble, limestone, ore calcite associated with magnetite skarn, fine-grained interstitial calcite, calcite from the late-stage retrograde alteration, and calcite from calcsilicate hornfels. The curve defines an inferred evolutionary trend from heavier oxygen and carbon isotope values in limestone and marble to lighter values in skarn, as the result of decarbonation and interaction of the infiltrating fluid. The box represents igneous carbonate (after [50]).

Table 3. Carbon and oxygen isotope data for calcite samples.

Sample	Description	δ^{13}C (% PDB)	δ^{18}O (% SMOW)
R76483	Limestone	3.9	19.0
R76477	Limestone	4.2	18.5
R76477	Limestone	3.5	15.1
R76467	Limestone	4.0	16.3
R76329	Marble	4.9	21.6
R76330	Marble	5.0	21.3
R76318	Marble	4.9	19.6
R76347	Ore assemblage calcite	−3.5	11.1
R76335	Ore assemblage calcite	−0.8	12.3
R76436	Ore assemblage calcite	−7.1	9.6
R76379	Ore assemblage calcite	−0.9	12.0
R76389	Ore assemblage calcite	−1.8	11.6
R76377	Late-stage alteration calcite	−3.9	18.6
R76363	Late-stage alteration calcite	−4.2	20.2
R76441	Late-stage alteration calcite	−1.9	20.5
R76364	Fine-grained calcite	−7.7	10.9
R76365	Fine-grained calcite	−6.1	12.6
R76468	Calc-silicate hornfels	−8.3	11.8
R76466	Calc-silicate hornfels	−5.7	14.4
R76488	Calc-silicate hornfels	3.4	12.0

δ^{18}*O in silicates*: The δ^{18}O values for magnetite and garnet are in the range of 7.6–10.4% and 2.4–4.4%, respectively (Table 4). The δ^{18}O values of the hydrous retrograde minerals (amphibole, epidote, and chlorite) range from 7.8 to 9.7%, 8 to 8.2%, and 0.2 to 4.1%, respectively. The oxygen isotope composition of the granite sample (9.5%) and the narrow range of granite quartz separates lie well within the range for I-type igneous rocks (e.g., [51]).

Using fractionation factors of Bottinga and Javoy (1973) for coexisting calcite and magnetite, which show equilibrium textures in the magnetite ore assemblage, temperatures of 572 °C and 604 °C were calculated for samples R76335 and R76379, respectively [52]. These temperatures are close to those estimated from the metamorphic assemblages [19] and measured in fluid inclusions.

δ*D in hydrous silicates*: Hydrous silicate minerals from the retrograde skarn assemblage and also biotite separates from the Degilbo Granite were analyzed both for oxygen and hydrogen isotopes (Table 4). For the retrograde skarn minerals, δD values cluster in a narrow range for each mineral; amphibole –117 to –132%, epidote –97 to –100%, chlorite –120 to –128%.

δ^{34}*S in sulfides*: The δ^{34}S values of all analyzed sulfides (molybdenite, bismuthinite, chalcopyrite, arsenopyrite, and pyrite) fall in the range of –5.6–2.3% and are comparable to the δ^{34}S values of sulfides in other skarn deposits (Table 5, Figure 12). The six pyrite samples have δ^{34}S values ranging from −5 to +2.3% with the maximum δ^{34}S value from pyrite in metamorphosed sedimentary rocks approximately 300 m outside the mine area.

Table 4. Oxygen and deuterium isotope data in silicates.

Sample	Mineral/Rock	δ^{18}O (%)	δD (%)	T °C [1]	δ^{18}O $_{H2O}$ (%) [2]	δD$_{H2O}$ (%)
R76296	Amphibole	8.6	−133	300–400	9.1 to 9.9	−63 to −81
R76331	Amphibole	7.8	−128	300–400	8.3 to 9.1	−58 to −77
R76388	Amphibole	9.7	−126	300–400	10.2 to 11	−56 to −75
R76430	Amphibole	8.1	−130	300–400	8.6 to 9.4	−60 to −79
R76435	Amphibole	8.7	−117	300–400	9.2 to 10	−48 to −66
R76463	Epidote	8.0	−100	300–400	5.9 to 7.4	−50
R76406	Epidote	8.2	−97	300–400	6.1 to 7.6	−47
R76302	Epidote	8.0	−98	300–400	5.9 to 7.4	−48
R76410	Biotite	6.2	−133	650	8.7	−99
R76344	Biotite	6.3	−128	650	8.8	−93
R76342	Biotite	5.7	−121	650	8.2	−87
R76338	Biotite	6.0	−114	650	8.5	−80
R76344	Granite	9.5	-	-	-	-
R76307	Chlorite	4.1	−120	310	4.2	−80
R76447	Chlorite	0.3	−122	310	0.4	−82
R76441	Chlorite	0.2	−128	310	0.3	−88
R76297	Garnet	9.2	-	550	11.1	-
R76335	Garnet	8.1	-	550	10.0	-
R76352	Garnet	8.2	-	550	10.1	-
R76358	Garnet	7.6	-	550	9.5	-
R76444	Garnet	10.4	-	550	12.3	-
R76379	Magnetite	4.4	-	550	10.3	-
R76427	Magnetite	3.6	-	550	9.5	-
R76335	Magnetite	2.8	-	550	8.7	-
R76353	Magnetite	2.4	-	550	8.3	-
R76410	Quartz	10.6	-	650	8.7	-
R76344	Quartz	10.0	-	650	8.1	-
R76342	Quartz	10.3	-	650	8.4	-
R76338	Quartz	10.4	-	650	8.5	-

[1] Based on fluid inclusions, mineral paragenesis, and chlorite thermometry. [2] Mineral-water fractionations of oxygen are calculated from Bottinga and Javoy (1973) [52] for amphibole and magnetite; Graham et al. (1980) [53] for epidote; Bottinga and Javoy (1973) [52] for biotite; Bottinga and Javoy (1975) [54] for garnet; Matsushisa et al. (1979) [55] for quartz; Wenner and Taylor (1971) [56] for chlorite. Mineral-water fractionations of hydrogen are calculated from Graham et al. (1984) [57] for amphibole; Graham et al. (1980) [53] for epidote; Suzuoki and Epstein (1976) [58] for biotite; and Kyser (1987 [59]: after Suzuoki and Epstein, 1976 [58]) for chlorite.

Table 5. Sulfur isotope data for sulfides from the Biggenden mine.

Sample	Mineral	δ^{34}S (% CDT)
R76375	Molybdenite	−1.6
R76378	Bismuthinite	−1.1
R76380	Bismuthinite	−1.1
R76524	Chalcopyrite	−1.1
R76430	Chalcopyrite	0.5
R76383	Arsenopyrite	−5.6
R76384	Arsenopyrite	1.4
R76385	Pyrite	−1.2
R76447	Pyrite	−5.0
R76376	Pyrite	−2.6
R76486	Pyrite	2.3
R76382	Pyrite	−1.0
R76381	Pyrite	−1.8

Strontium isotopes: In order to use the Sr data (Table 6) as hydrothermal tracers and compare the results in different rock types, the initial ^{87}Sr/^{86}Sr ratios have been calculated for the age of the Degilbo Granite (215 Ma). A comparison of the Sr isotope values of ore-stage calcite samples to the nearby rocks (Figure 13) shows that the ^{87}Sr/^{86}Sr ratio in calcite has a narrow range and is lower than that in limestone and metasiltstone and higher than that in the Degilbo Granite. One sample from metavolcanic rock with a higher

^{87}Sr/^{86}Sr ratio is from the mine (R76402, Table 6), and its strontium isotope composition may have been modified during fluid/rock interaction. The other sample (R76501, Table 6) collected outside the mine area is a metabasalt.
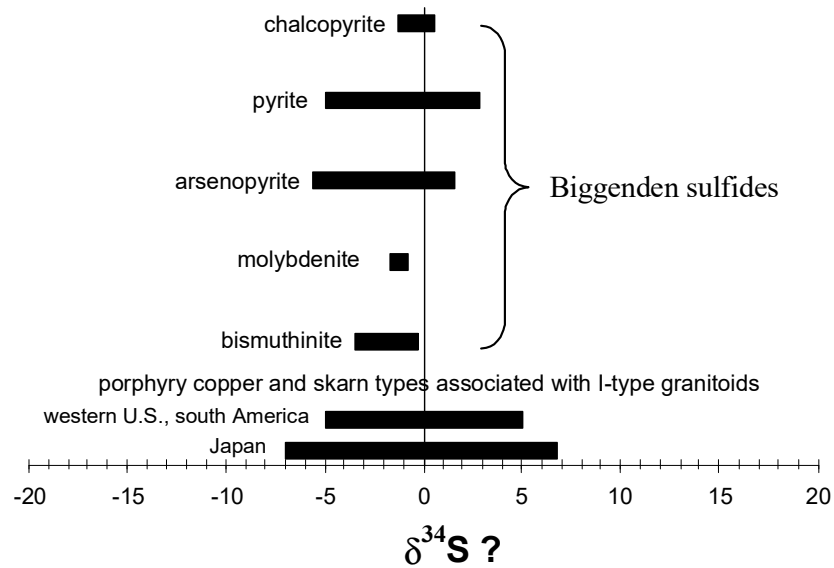

Figure 12. Sulfur isotope composition of the Biggenden sulfides compared to those of other skarn deposits in the world (data from [60]).

Table 6. Strontium isotope data for rocks from the Biggenden mine.

| Sample	Description	^{87}Rb/^{86}Sr	^{87}Sr/^{86}Sr	^{87}Sr/^{86}Sr initial	Sr ppm	Rb ppm
R76472	Metasiltstone	1.9483	0.7128	0.70684	169	114
R76402	Metavolcanic	0.2352	0.7062	0.70548	442	36
R76501	Metavolcanic	0.0593	0.7034	0.70322	341	7
R76410	Granite	2.2000	0.7106	0.70387	256	195
R76344	Granite	2.6346	0.7121	0.70404	205	187
R76483	Limestone	0.0543	0.7065	0.70633	319	6
R76502	Ore assemblage calcite	0.0245	0.7047	0.70463	118	<1
R76335	Ore assemblage calcite	0.0162	0.7046	0.7046	178	<1
R76357	Ore assemblage calcite	0.0222	0.7048	0.70473	130	<1
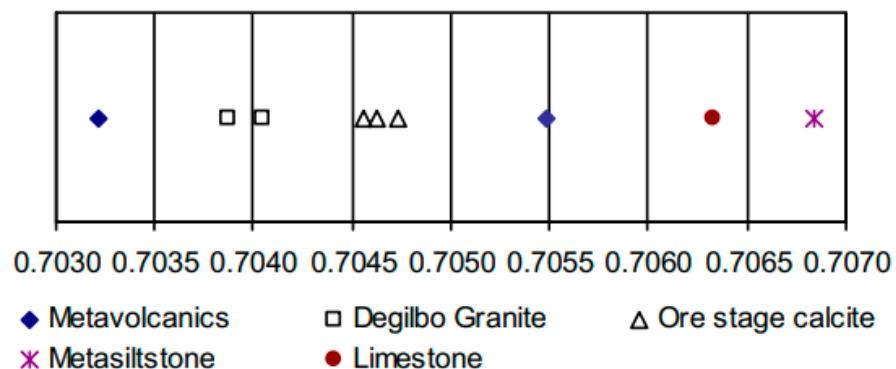
Figure 13. Plot of ^{87}Sr/^{86}Sr isotope ratios for different rocks in the Biggenden area compared to those of three ore-stage calcite samples from the Biggenden mine.

Lead isotopes: Lead isotope data for two galena samples were measured on polished thin sections by in situ analysis. The analyzed galena grains belong to sulfide-bearing retrograde assemblages that formed at lower temperatures (300–400 °C) than the prograde skarn minerals. The Biggenden galena samples have a narrow range of Pb isotope values

and have ^{206}Pb/^{204}Pb, ^{207}Pb/^{204}Pb, and ^{208}Pb/^{204}Pb ratios that are similar to those of other hydrothermal deposits associated with Triassic intrusions in southeast Queensland (Figure 14; Table 7). The measured values are initial ratios because the U/Pb and Th/Pb ratios of galena are so low that isotopic ratios do not change significantly with time [61].
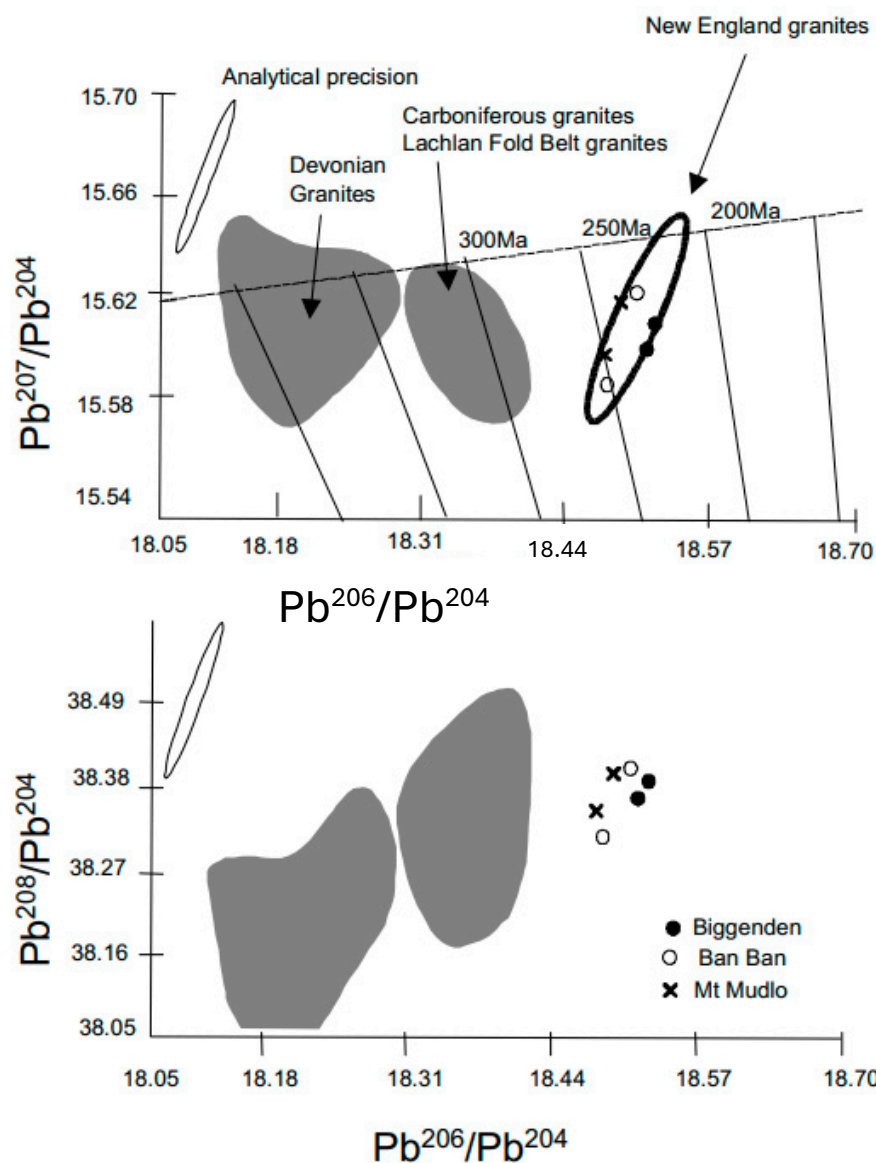
Figure 14. Lead isotope ratios for galena samples from the Biggenden mine and two other deposits (Ban Ban Zn skarn and Mt Mudlo mesothermal Cu-Mo-W vein) related to the Triassic granitoids in southeast Queensland. Fields for Devonian and Carboniferous granites from the Lachlan Fold Belt of eastern Australia are from [62]. New England Orogen granite ellipse from G. Carr (unpublished data).

Table 7. Pb isotope data for Biggenden galena and two other hydrothermal deposits associated with the Triassic granitoids in the area [15].

Location	Sample	^{206}Pb/^{204}Pb	^{207}Pb/^{204}Pb	^{208}Pb/^{204}Pb
Biggenden	R76448	18.505	15.602	38.369
	R76441	18.514	15.613	38.391
Ban Ban	BB1	18.472	15.589	38.315
	BB3	18.495	15.625	38.406
Mt Mudlo	MM22	18.466	15.602	38.350
	MM44A	18.480	15.620	38.401

5. Discussion

5.1. Isotope Interpretations

The δ^{13}C and δ^{18}O values are relatively high in Biggenden marbles (Figure 11) and are similar to those of marbles elsewhere (e.g., [63]). Skarn calcite samples isotopically resemble calcite in other skarn deposits [64–66] and display a trend towards lighter δ^{13}C and δ^{18}O values compared to those of marble and limestone. Similar depletion trends have been reported for other skarn deposits worldwide [50], with initial limestone in the range of δ^{18}O = 20 to 25% and δ^{13}C = −2 to 5%, and final skarn calcite values near igneous values (Figure 11). This depletion can result either from the evolution of CO_2 during decarbonation or from the interaction with infiltrating fluid (e.g., [67]). Metamorphic decarbonation preferentially removes heavy isotopes through the loss of CO_2 (e.g., [68]), although the maximum decrease in δ^{18}O by this mechanism in marbles is 2%. A large decrease in δ^{18}O values in marbles and low δ^{13}C values in skarn calcite has been interpreted in other skarns to be the result of water-rock exchange or infiltration metasomatism from multiple fluid sources mainly involving magmatic-hydrothermal fluids (e.g., [69]).

The isotopic composition of late-stage calcite is similar to that in some late-stage open space-filling calcite in other skarn deposits (e.g., [70]). Heavy δ^{18}O values for late-stage calcite may indicate the interaction of magmatic fluids with more ^{18}O-enriched sediments during skarn formation. The δ^{13}C values for the calc-silicate hornfels are lower than those in the limestone samples and likely reflect the involvement of metasomatic fluids.

A good correlation between the δ^{18}O values of calcite from skarns and the whole rock values of the associated plutons has been cited as evidence for the likely magmatic origin of most skarn-forming fluids (e.g., [71]). The δ^{18}O value of Degilbo Granite and the mean value for skarn calcite are aligned with the correlation trend of Nabelek (1991) [71]. Moreover, the calculated δ^{18}O of the metasomatic fluid in equilibrium with the skarn calcite at 500 °C (8.4–11%) (fractionation factors from Friedman and O'Neil, 1977 [72]) is close to that calculated for the fluid in equilibrium with the granite and anhydrous skarn silicates (Table 4).

The oxygen isotope composition of magnetite at Biggenden (2.4–4.4%) is similar to that in other Fe skarn deposits (e.g., Iron Hat skarn [73] and Peña Colorada deposit [74]). The range of oxygen isotope composition (8.1 to 10.4%) in the Biggenden garnet is similar to that in some gold skarns (e.g., Fortitude deposit [8]).

The δ^{18}O values for the fluid in equilibrium with skarn minerals as well as mineral separates from the granite have been calculated for the related temperature ranges (Figure 15). In these calculations, a temperature of 550 °C has been used for prograde garnet and magnetite. This temperature estimate is based on fluid inclusion studies, isotope thermometry, and contact metamorphic assemblages of the hornblende-hornfels facies. A temperature of 650 °C was used in the calculations for the quartz and biotite separates from the Degilbo Granite, assuming that these minerals formed at this temperature during the crystallization of the granitic melt. The 300–400 °C temperature used for amphibole and epidote is based on the paragenetic relationship of these minerals in the retrograde assemblages, which formed earlier than chlorite and probably at slightly higher temperatures. Fluid inclusion studies in quartz associated with chlorite and thermometry based on the chemical composition of chlorite [39] indicate that chlorite formed at average temperatures of 310 °C.

The δ^{18}O values of fluid in equilibrium with garnet and amphibole are slightly heavier than the δ^{18}O of fluids in many skarn deposits associated with felsic magmatic rocks [75]. This could be due to the effect of fluid/rock interaction; granitoid-derived fluids interacted with more ^{18}O-enriched sediments during skarn formation. However, the oxygen isotopic values of the fluid in equilibrium with chlorite in the retrograde assemblage are lower, and meteoric water is a more likely source for this fluid. The range of δ^{18}O values for epidote

could also indicate the involvement of meteoric water. The general decreasing trend of the $\delta^{18}O$ in fluid from 8.0 to 3.0% has been attributed in other skarn deposits to the mixing of magmatic fluid with meteoric water (e.g., [67]).
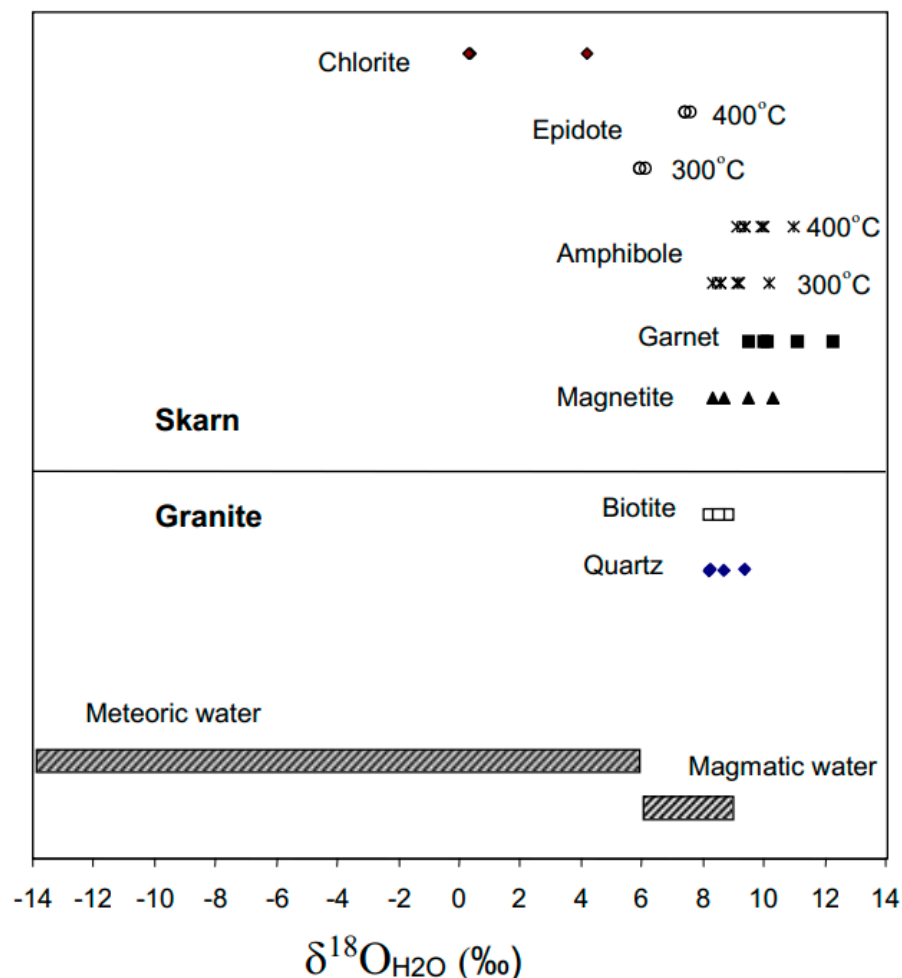
Figure 15. Calculated $\delta^{18}O$ values for the fluids in equilibrium with the skarn minerals and mineral separates from the Degilbo Granite (see Table 4). The range for magmatic and meteoric waters is from [68].

Biotite from the Degilbo Granite has δD values (-114 to -133%, Figure 16, Table 4) that suggest equilibrium with magmatic water of $\delta D = -80$ to -99% (using the fractionation factors of Suzuoki and Epstein 1976 [58]). The δD values of biotite do not show systematic changes with distance from the igneous contact that could infer the mixing of magmatic waters with the meteoric waters. This is also supported by field and petrological evidence that the Degilbo Granite has not interacted significantly with the hydrothermal fluids. An effect of imposed weathering on the δD values of biotite is unlikely as the analyzed samples are quite fresh. The involvement of meteoric water that would be highly depleted in D, however, could be explained by the geographic position of this part of eastern Australia in Triassic time at a latitude of 50–55° S [76,77].
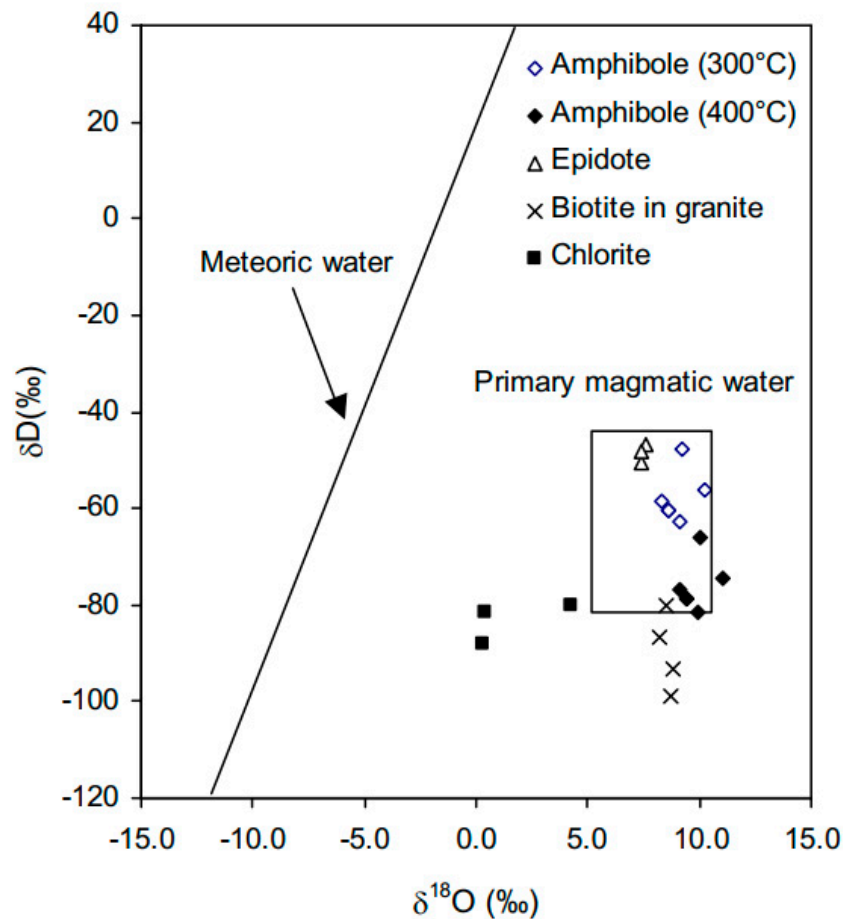
Figure 16. Calculated $\delta^{18}O$ versus δD diagram for fluids at temperatures in the range of 300–550 °C in equilibrium with skarn minerals and biotite samples from granite (see Table 4). The field for magmatic water and the line for meteoric waters are from [78].

Amphibole samples have δD values of −133 to −126‰, which is consistent with the contribution of meteoric water during the retrograde stage. Similarly, the isotopic composition of water in equilibrium with chlorite samples at 310 °C (fractionation factors from Taylor and O'Neil, 1977 [79]) is lighter and may suggest the presence of meteoric water during the retrograde skarn formation. In contrast, the δD values of water in equilibrium with the amphibole samples at 300–400 °C range between −48 and −81‰, which is consistent with δD for magmatic water. Although the $\delta^{18}O$ values of fluid in equilibrium with epidote show a slight shift towards the meteoric water composition, δD values for these fluids (−47 to −50‰ based on fractionation factors from Graham et al., 1980 [53]) are close to magmatic values. It is not clear to what extent the early prograde magmatic fluid was mixed with highly depleted meteoric water during the retrograde alteration, but the chlorite oxygen values show a significant contribution of meteoric water at the retrograde stage.

The sulfur isotope values of Biggenden sulfides are in the range of those for other magnetite-bearing skarn deposits and have been attributed to a magmatic origin (e.g., [2,60,80]). In terms of the Sr isotope values (Figure 12), the intermediate position of the ore-stage calcite between igneous rocks (Degilbo Granite and metabasalt) and sedimentary units (limestone and metasiltstone) may indicate that both the Degilbo Granite and the Gympie Group rocks supplied Sr to the hydrothermal fluid. The low initial $^{87}Rb/^{86}Sr$ ratios of the Degilbo Granite (0.70387–0.70404) are comparable to those of I-type granites (e.g., [22,23]). The lead isotope ratio suggests a model age of ~225 Ma for mineralization (Figure 14), which is consistent with the age proposed for the Degilbo Granite [15]. The lead isotope data also lie below the Cumming and Richards (1975) [81] growth curve, suggesting

a mantle contribution to the ore Pb. Mantle Pb could have been derived from the Degilbo Granite, which is an I-type pluton, or by leaching of Pb from the Gympie Group basalts.

5.2. Classification of the Biggenden Skarn Deposit

Based on mineralogy and dominant metals present, the Biggenden deposit is a gold-bearing iron skarn [3,25]. Skarn deposits containing economic concentrations of magnetite are found in post-orogenic terrains similar to Biggenden and are associated with Fe-rich plutons [1]. However, Biggenden is different from typical island arc calcic magnetite skarn deposits, as they are usually associated with relatively primitive plutons and show widespread sodium metasomatism [1,3].

Biggenden has been mined for gold in the past, and it has common features with gold skarns. These common features include the presence of biotite hornfels, garnet-pyroxene alteration, clastic or volcaniclastic-rich protoliths, As and Bi minerals, and association with a shallow-level, silicic, magnetite-bearing pluton. Characteristics such as high ratios of garnet/pyroxene, low total sulfides, high abundance of pyrite, lack of pyrrhotite, minor occurrence of chalcopyrite and galena, and the presence of a pyrite and magnetite assemblage are all consistent with gold skarns, except that garnets are Fe-rich in Biggenden [82].

The average composition of the Degilbo Granite is higher in SiO_2 (68.5%) and K_2O (4.18%) and lower in MgO (0.9%) compared to plutons typically associated with Fe skarns (Figure 9). It is a weakly oxidized pluton and has an average $Fe_2O_3/Fe_2O_3 + FeO$ ratio similar to plutons typically associated with Fe skarns (Figure 9). The Degilbo Granite has lower average values of Ni (5 ppm), Cr (9 ppm), V (34 ppm), and Sc (9 ppm) and also contains on average more Zr (270 ppm), Rb (176 ppm), Ba (694 ppm), and Sc (9 ppm) than plutons commonly associated with Fe skarns (Figure 9), which suggests that the Degilbo Granite crystallized from more fractionated magmas. It also has higher Rb/Sr (0.7) ratios than plutons associated with Fe-skarns (Figure 9). The major and trace element content of the Degilbo Granite is intermediate between the Fe-Cu-Au group and the Sn-W-Mo group of skarn-forming granitoids [3,82,83].

Garnet and pyroxene compositions from the Biggenden mine are analogous to those in several gold skarn deposits, particularly Nambija, Ecuador, and McCoy, Nevada [8]. The presence of Cl-rich scapolite in Biggenden is similar to both iron and gold skarn deposits (e.g., [36,84–86]).

Distribution of homogenization temperature data in the prograde-high temperature and retrograde-low temperature assemblages is common in iron skarns (e.g., Iron Hat [73]; Vyhne-Klokoc [87]). Moderate to high salinities and high homogenization temperatures in Biggenden are also similar to some gold skarn deposits [8].

In summary, in terms of ore mineralization, Biggenden is a gold-bearing iron skarn deposit. However, the associated granitic body, Degilbo Granite, at the exposed level is more fractionated, felsic, and oxidized than granites associated with common iron deposits. As a result, in terms of associated pluton, this deposit shows some similarities with Au and even the Sn-W-Mo group of skarn-forming granitoids.
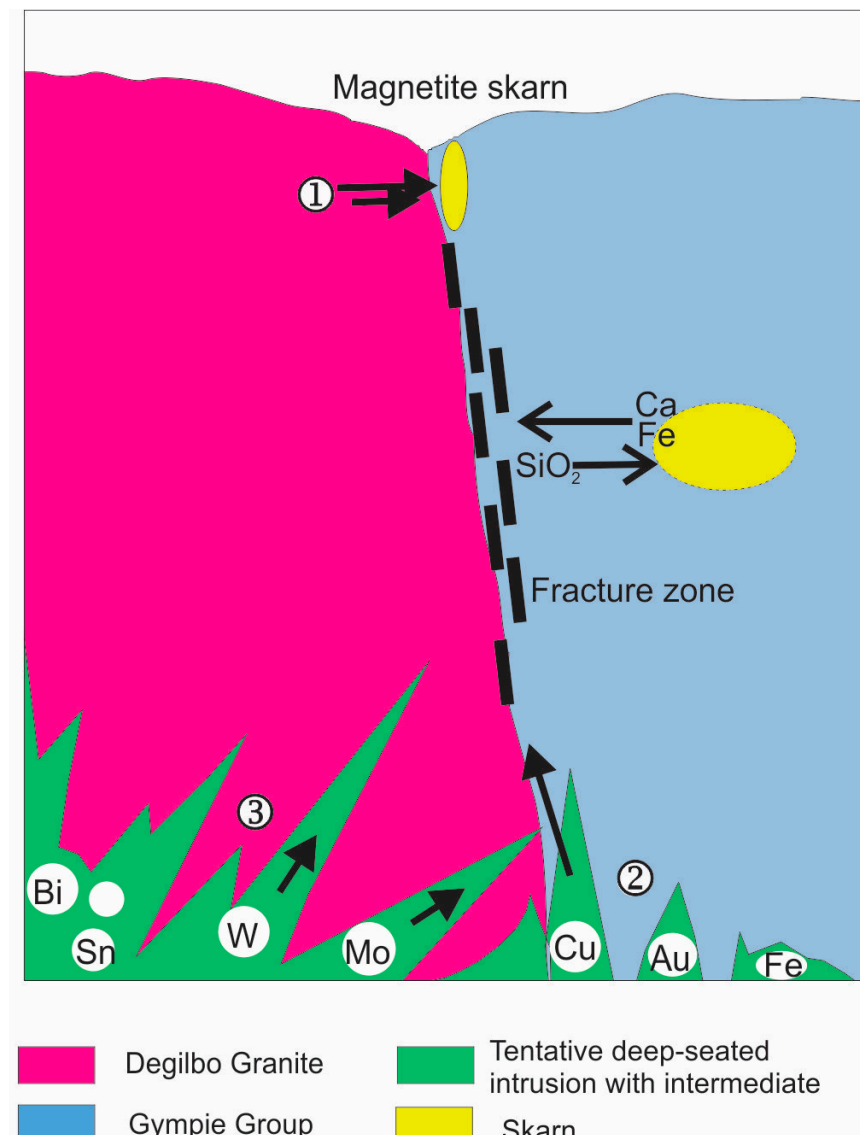
5.3. Genetic Models

The spatial association of the Biggenden deposit with the Degilbo Granite may suggest that the ore-bearing fluids were derived directly from the adjacent pluton (model 1, Figure 17). Field evidence such as the scarcity of fracture systems and veins, lack of any significant structures that could act as fluid pathways, lack of greisen, and the general absence of endoskarn replacement in the granite may imply that there has been little infiltration across the contact into the pluton. The geochemical characteristics of the Degilbo Granite are analogous to those in intrusions associated with Fe-Cu-Au skarns as well as those

associated with other skarn types. The presence of Cu and Au in the orebody suggests that there may be a genetic link between skarn mineralization and a deep-seated intermediate intrusion (perhaps of porphyry Cu-Au type) that provided some of the ore constituents, including Fe, Cu, and Au (model 2, Figure 17). It is noteworthy that a porphyry Cu system (Coalstoun deposit) is hosted by an early Triassic tonalitic intrusion in the district [88]. The formation of skarns from hidden intrusions has been suggested by other workers (e.g., [89–91]). There is, however, no field evidence (such as near-surface dikes) that could imply the presence of another pluton at depth.

Field relations, such as the proximity of ore deposition to a shear zone, numerous faults, and steeply dipping volcanic and sedimentary host rocks, suggest that the hydrothermal fluids responsible for skarn formation have most likely risen from depth along structural zones and sedimentary layer boundaries, rather than passing directly across the intrusive contact.

Figure 17. Possible genetic models proposed for the formation of magnetite skarn at the Biggenden mine. Metasomatism of SiO_2, Ca, and Fe is shown schematically. Numbers refer to the potential sources of metals.

Geochemical studies of the orebody [19] show that "granitophile" elements Sn, W, Mo, and Bi are enriched. In addition, a genetic link between skarn mineralization and the em-

placement of the Degilbo Granite is, to some extent, supported by isotopic evidence. Skarn calcite has $\delta^{13}C$ and $\delta^{18}O$ values, which indicate deposition from magmatically derived fluids with isotopic compositions similar to that calculated for the fluid in equilibrium with the Degilbo Granite. Moreover, the calculated $\delta^{18}O$ values of the fluid in equilibrium with the skarn magnetite and amphibole are in the range of those for biotite and quartz from the Degilbo Granite. Lead and strontium isotope data also support a third genetic model, which involves both the Degilbo Granite and the Gympie Group.

The inconsistencies between the geochemical evidence (which suggests the role of the Degilbo Granite in the ore genesis) and the field evidence (that does not clearly support a direct genetic link between granite and skarn) can be explained by assuming that the Degibo Granite is in fact the source of hydrothermal fluids and metals but not at the current level of exposure. In our preferred model, hydrothermal fluids emanating from the Degilbo Granite at depth may have been channeled by the shear zone, intrusive contact, and through permeable Gympie Group rocks, reacted with adjacent marble and basalt, and deposited magnetite both as replacement bodies and as vein and breccia fillings. High-temperature and high-salinity fluids at Biggenden, similar to other Au-skarns [3,8], can transport significant amounts of gold as chloride complexes. This would allow a long-distance (and large-volume) metasomatic equilibration with low-Si and high-Fe rocks of the Gympie Group, leading to desilication of originally magmatic fluids and their enrichment in Fe and Ca (model 3, Figure 17).

6. Conclusions

- The Biggenden Gold-Bearing Fe Skarn is a calcic magnetite skarn type that is hosted by the Early Permian volcanic and sedimentary rocks of the Gympie Group due to the intrusion of the Late Triassic Degilbo Granite.
- The skarn mineralogy varies from the prograde garnet, clinopyroxene, magnetite, and scapolite to retrograde epidote and ferropargasite, followed by chlorite, calcite, actinolite, quartz, sulfides, gold, nontronite, and quartz.
- The prograde mineralization occurred at a high temperature (500–600 °C) from high salinity (up to 45 equivalent wt % NaCl) hydrothermal fluids. Lower temperatures (280–360 °C) and lower salinity (5–15 equivalent wt % NaCl) solutions precipitated the retrograde sulfide minerals.
- The $\delta18O$ values of the fluids indicate that the prograde minerals were precipitated from magmatic water, whereas the retrograde minerals were mainly deposited from a meteoric fluid. Sulfur was likely derived from a magmatic source.
- Sr and Pb isotopes suggest that the volcanic and sedimentary rocks of the Gympie Group may have partially provided the metals to the hydrothermal solution.

Conflicts of Interest: The authors declare no conflicts of interest.

References

1. Einaudi, M.T.; Meinert, L.D.; Newberry, R.J. Skarn deposits. *Econ. Geol.* **1981**, *75*, 317–391.
2. Meinert, L.D. Skarns and skarn deposits. *Geosci. Can.* **1992**, *19*, 145–162.
3. Meinert, L.D.; Dipple, G.M.; Nicolescu, S. World Skarn Deposits. In *Economic Geology*; Hedenquist, J.W., Thompson, J.F.H., Goldfarb, R.J., Richards, J.P., Eds.; Society of Economic Geologists: Littleton, CO, USA, 2005; 100th Anniversary Volume, pp. 299–336.
4. Ren, L.; Huang, J.; Wang, X.; Yang, S.; Yang, C.; Zhao, C.; Wang, L.; Mei, W.; Deng, M.; Zhou, Y. Magmatic control on orebody distribution of porphyry-skarn gold-copper deposit: A case study of Beiya deposit from Sanjiang metallogenic belt in the southwest China. *Ore Geol. Rev.* **2024**, *175*, 106350. [CrossRef]
5. Sui, J.X.; Li, J.W.; Wen, G.; Jin, X.Y. The Dewulu reduced Au-Cu skarn deposit in the Xiahe-Hezuo district, West Qinling orogen, China: Implications for an intrusion-related gold system. *Ore Geol. Rev.* **2017**, *80*, 1230–1244. [CrossRef]
6. Zhou, H.; Sun, X.; Wu, Z.; Huang, Q. Timing of skarn gold deposition in the giant Beiya polymetallic gold deposit, southwest China: Constraints from in situ monazite SIMS U-Th-Pb geochronology. *Ore Geol. Rev.* **2019**, *106*, 226–237. [CrossRef]
7. Weekes, G. Biggenden magnetite mine, assessment of reserves March 1992 and preliminary proposal for final development, Commercial Minerals. 1992; Unpublished report No. 5/92. Brisbane, Queensland, Australia.
8. Meinert, L.D. A review of skarns that contain gold. *Mineral. Assoc. Can. Short Course Ser.* **1988**, *26*, 359–414.
9. Seccombe, P.K.; Downes, P.M.; Ashley, P.M.; Brathwaite, R.L.; Green, G.R.; Murray, C.G.; Rubenach, M.J. World Skarn Deposits: Skarns of the Southwest Pacific. In *Economic Geology*; Hedenquist, J.W., Thompson, J.F.H., Goldfarb, R.J., Richards, J.P., Eds.; Society of Economic Geologists: Littleton, CO, USA, 2005; 100th Anniversary Volume, pp. 299–336.
10. Clarke, D.E. The Geology of the Mount Biggenden Gold and Bismuth Mine and Environs. Unpublished Bachelor's Thesis, University of Queensland, Brisbane, Australia, 1963; p. 137.
11. Clarke, D.E. *Geology of the Mount Biggenden Gold and Bismuth Mine and Environs*; Report nr. 32; Geological Survey of Queensland: Brisbane, Australia, 1 January 1969; p. 16.
12. Tellam, L. Geology of the Mt. Biggenden Magnetite Mine Environs, Southeast Queensland, Geochemical and Mineralogical Aspects. Unpublished Bachelor's Thesis, University of Queensland, Brisbane, Australia, 1980; p. 71.
13. Li, P.; Rosenbaum, G.; Yang, J.; Hoy, D. Australian-derived detrital zircons in the Permian-Triassic Gympie terrane (eastern Australia): Evidence for an autochthonous origin. *Tectonics* **2015**, *34*, 858–874. [CrossRef]
14. Holcombe, R.J.; Stephens, C.J.; Fielding, C.R.; Gust, D.; Little, A.; Sliwa, R.; Kassan, J.; McPhie, J.; Ewart, A. Tectonic evolution of the northern New England fold belt: The Permian-Triassic Hunter-Bowen event. In *Tectonics and Metallogenesis of the New England Orogen*; Ashley, P.M., Flood, P.G., Eds.; Geological Society Special Publication: London, UK, 1997; Volume 19, pp. 52–65.
15. Cranfield, L.C. *1: 250,000 Geological Series-Explanatory Notes, Maryborough*; Queensland Sheet SG56-6; Department of Minerals and Energy: Brisbane, Australia, 1994; p. 120.
16. Jell, P.A.; Cranfield, L.C. Gympie Province. In *Geology of Queensland*; Jell, P.A., Ed.; Geological Survey of Queensland: Brisbane, Australia, 2013; pp. 369–371.
17. Sivell, W.J.; Waterhouse, J.B. Petrogenesis of Gympie Group volcanics; evidence for remnants of an Early Permian volcanic arc in eastern Australia. *Lithos* **1988**, *21*, 81–95. [CrossRef]
18. Hoy, D.; Rosenbaum, G. Episodic behavior of Gondwanide deformation in eastern Australia: Insights from the Gympie Terrane. *Tectonics* **2017**, *36*, 1497–1520. [CrossRef]
19. Edraki, M. Geochemistry, Mineralogy and Genesis of the Biggenden Au-Bi-Fe Skarn Deposit, Southeast Queensland, Australia. Unpublished Ph.D. Thesis, University of New England, Armidale, Australia, 2000; p. 318.
20. Cranfield, L.C.; Murray, C.G. Geochemistry and tectonic setting of granitic rocks in the Maryborough 1:250 000 sheet area, Southeast Queensland—Caractéristiques géochimiques et tectoniques des roches granitiques sur la feuille au 1:250 000 de Maryborough, SE de Queensland. *Queensl. Gov. Min. J.* **1989**, *90*, 408–415.
21. Webb, A.W.; McDougall, I. Isotopic dating evidence on the age of the Upper Permian and Middle Triassic. *Earth and Planetary Sci. Lett.* **1967**, *2*, 483–488. [CrossRef]
22. Chappell, B.W.; White, A.J.R. I- and S-type granites in the Lachlan Fold Belt. *Trans. R. Soc. Edinb. Earth Sci.* **1992**, *83*, 1–26.
23. Chappell, B.W.; White, A.J.R. Two contrasting granite types: 25 years later. *Aust. J. Earth Sci.* **2001**, *48*, 489–499. [CrossRef]
24. Cobine, T.J. The Analytic Signal and Cross-Correlation Applied in Rapid, Detailed Analysis of Aeromagnetic and Radiometric Data. Unpublished Master's Thesis, University of New England, Armidale, Australia, 1997; p. 75.
25. Roedder, E. Fluid inclusions. *Rev. Mineral.* **1984**, *12*, 644.
26. Clayton, R.N.; Mayeda, T.K. The use of bromine pentafluoride in the extraction of oxygen from oxides and silicates for isotopic analysis. *Geochem. Cosmochim. Acta* **1963**, *27*, 43–52. [CrossRef]
27. Friedman, I. Deuterium content of natural waters. *Geochim. Cosmochim. Acta* **1953**, *4*, 89–103. [CrossRef]

28. Robinson, B.W.; Kusakabe, M. Quantitative preparation of sulfur dioxide for ^{34}S/^{32}S analysis from sulfides by combustion with cuprous oxide. *Anal. Chem.* **1975**, *47*, 1179–1181. [CrossRef]

29. McCrea, J.M. The isotope geochemistry of carbonates and a paleotemperature scale. *J. Chem. Phys.* **1950**, *18*, 849–857. [CrossRef]

30. Sies, S.H.; Niklaus, T.R.; Sims, D.A.; Bruhn, F.; Suter, G.; Cripps, G. AUSTRALIS: A new tool for the study of isotopic systems and geochronology in mineral systems. *Aust. J. Earth Sci.* **2002**, *49*, 601–611.

31. Theodore, T.G.; Orris, G.J.; Hammarstrom, J.M.; Bliss, J.D. *Gold-Bearing Skarns*, 1930th ed.; U.S. Government Printing Office: Washington, DC, USA, 1991; pp. 1–35.

32. Nakano, T.; Yoshino, T.; Shimazaki, H.; Shimizu, M. Pyroxene composition as an indicator in the classification of skarn deposits. *Econ. Geol.* **1994**, *89*, 567–1580. [CrossRef]

33. Matsueda, H. Pyrometasomatic iron-copper ore deposits of the Sampo Mine, Okayama Prefecture; II, The modes of occurrences, mineral paragenesis and chemical compositions of skarn and ore. *Min. Geol.* **1981**, *6*, 1–43.

34. Einaudi, M.T.; Burt, D.M. Introduction—Terminology, classification, and composition of skarn deposits. *Econ. Geol.* **1982**, *77*, 745–754. [CrossRef]

35. Meinert, L.D. Gold skarn deposits–geology and exploration criteria. *Econ. Geol.* **1989**, *65*, 537–552.

36. Pan, Y. Scapolite in skarn deposits; petrogenetic and geochemical significance. *Mineral. Assoc. Can. Short Course Handb.* **1998**, *26*, 169–210.

37. Pan, Y.; Fleet, M.E.; Ray, G.E. Scapolite in two Canadian gold deposits: Nickel Plate British Columbia and Hemlo. *Ontario Can. Mineral.* **1994**, *32*, 825–837.

38. Meinert, L.D. Mineralogy and petrology of iron skarns in western British Columbia, Canada. *Econ. Geol.* **1984**, *79*, 869–882. [CrossRef]

39. Cathelineau, M. The chlorite and illite geothermometers. *Chem. Geol.* **1988**, *70*, 182–183. [CrossRef]

40. Le Bas, M.J.; Streckeisen, A.L. The IUGS systematics of igneous rocks. *J. Geol. Soc. Lond.* **1991**, *148*, 825–833. [CrossRef]

41. Peccerillo, A.; Taylor, S.R. Geochemistry of Eocene calc-alkaline volcanic rocks from the Castamoun area, northern Turkey. *Contrib. Mineral. Petrol.* **1976**, *58*, 63–81. [CrossRef]

42. Kwak, T.A.P. Fluid inclusions in skarns (carbonate replacement deposits). *J. Metamorph. Geol.* **1986**, *4*, 363–384. [CrossRef]

43. Kwak, T.A.P.; Tan, T.H. The geochemistry of zoning in skarn minerals at the King Island (Dolphin) Mine. *Econ. Geol.* **1981**, *76*, 468–497. [CrossRef]

44. Meinert, L.D. Skarn zonation and fluid evolution in the Groundhog Mine, Central mining district, New Mexico. *Econ. Geol.* **1987**, *82*, 523–545. [CrossRef]

45. Potter, R.W.; Clynne, M.A.; Brown, D.L. Freezing point depression of aqueous sodium chloride solutions. *Econ. Geol.* **1978**, *73*, 284–285. [CrossRef]

46. Bodnar, R. Revised equation and table for determining the freezing point depression of H_2O-Nacl solutions. *Geochim. Cosmochim. Acta* **1993**, *57*, 683–684. [CrossRef]

47. Lentz, D.R. Carbonatite genesis: A reexamination of the role of intrusion-related pneumatolytic skarn processes in limestone melting. *Geology* **1999**, *27*, 335–338. [CrossRef]

48. Xu, X.; Xu, X.; Szmihelsky, M.; Yan, J.; Xie, Q.; Steele-MacInnis, M. Melt inclusion evidence for limestone assimilation, calc-silicate melts, and "magmatic skarn". *Geology* **2023**, *51*, 491–495. [CrossRef]

49. Ohmoto, H. Stable isotope geochemistry of ore deposits. In *Stable Isotopes in High Temperature Geological Processes*; Valley, J.W., Taylor, H.P., O'Neil, J.R., Eds.; Mineralogical Society of America: Chantilly, VA, USA, 1986; Volume 16, pp. 491–559.

50. Valley, J.W. Stable isotope geochemistry of metamorphic rocks. *Rev. Mineral.* **1986**, *16*, 445–489.

51. Taylor, H.P.; Sheppard, S.M.F. Igneous rocks, I. Processes of isotopic fractionation in isotope systematics. *Rev. Mineral.* **1986**, *16*, 227–271.

52. Bottinga, Y.; Javoy, M. Comments on oxygen isotope geothermometry. *Earth Planet. Sci. Lett.* **1973**, *20*, 250–265. [CrossRef]

53. Graham, C.M.; Sheppard, S.M.F.; Heaton, T.H.E. Experimental hydrogen isotope studies—I. Systematics of hydrogen isotope fractionation in the systems epidote-H_2O, zoisite-H_2O and AlO(OH)-H_2O. *Geochimica Cosmochimica Acta* **1980**, *44*, 353–364. [CrossRef]

54. Bottinga, Y.; Javoy, M. Oxygen isotope partitioning among the minerals in igneous and metamorphic rocks. *Rev. Geophys.* **1975**, *13*, 401–418. [CrossRef]

55. Matsushisa, Y.; Goldsmith, N.; Tanaka, T. Oxygen isotope fractionation in the system quartz-albite-anorthite-water. *Geochim. Cosmochim. Acta* **1979**, *43*, 1131–1140. [CrossRef]

56. Wenner, D.B.; Taylor, H.P., Jr. Temperatures of serpentinization of ultramafic rocks based on ^{18}O/^{16}O fractionation between coexisting serpentine and magnetite. *Contrib. Mineral. Petrol.* **1971**, *32*, 165–185. [CrossRef]

57. Graham, C.M.; Harmon, R.S.; Sheppard, S.M.F. Experimental hydrogen isotope studies, hydrogen isotope exchange between amphibole and water. *Am. Mineral.* **1984**, *69*, 128–138.

58. Suzuoki, T.; Epstein, S. Hydrogen isotope fractionation between OH-bearing minerals and water. *Geochim. Cosmochim. Acta* **1976**, *40*, 1229–1240. [CrossRef]

59. Kyser, T.K. Equilibrium fractionation factors for stable isotopes. In *Stable Isotope Geochemistry of Low Temperature Processes*; Mineralogical Association of Canada: Montreal, QC, Canada, 1987; Volume 13, pp. 1–84.

60. Ohmoto, H.; Goldhaber, M.B. Sulfur and carbon isotopes. In *Geochemistry of Hydrothermal Ore Deposits*, 3rd ed.; Barnes, H.L., Ed.; John Wiley and Sons: New York, NY, USA, 1997; pp. 517–612.

61. Faure, G. *Principles of Isotope Geology*, 2nd ed.; John Wiley and Sons: New York, NY, USA, 1986; p. 589.

62. Carr, G.R.; Dean, J.A.; Suppel, D.W.; Heithersay, P.S. Precise lead isotope fingerprinting of hydrothermal activity associated with Ordovician to Carboniferous metallogenic events in the Lachlan Fold Belt of New South Wales. *Econ. Geol.* **1995**, *90*, 1467–1505. [CrossRef]

63. Cartwright, I.; Weaver, T.R. Fluid-rock interaction between syenites and marbles at Stephen Cross Quarry, Québec, Canada: Petrological and stable isotope data. *Contrib. Mineral. Petrol.* **1993**, *113*, 533–544. [CrossRef]

64. Baker, T.; Lang, J.R. Reconciling fluid inclusions, fluid processes and fluid source in skarns: An example from the Bismarck skarn deposit, Mexico. *Miner. Depos.* **2003**, *38*, 474–495. [CrossRef]

65. Bowman, J.R. Stable-isotope systematics of skarns. *Mineral. Assoc. Can. Short Course Ser.* **1998**, *26*, 99–145.

66. Bowman, J.R.; O'Neil, J.R.; Essene, E.J. Contact skarn formation at Elkhorn, Montana. *II: Origin and evolution of C-O-H skarn fluids.* *Am. J. Sci.* **1985**, *285*, 621–660.

67. Vander-Auwera, J.; Andre, L. Trace elements (REE) and isotopes (O, C, Sr) to characterize the metasomatic fluid sources: Evidence from the skarn deposit (Fe, W, Cu) of Traversella (Ivrea, Italy). *Contrib. Mineral. Petrol.* **1991**, *106*, 325–339. [CrossRef]

68. Taylor, B.E. Stable isotope geochemistry of ore-forming fluids. *Mineral. Assoc. Can. Short Course Handb.* **1987**, *13*, 377–445.

69. Zaw, K.; Singoyi, B. Formation of Magnetite-Scheelite Skarn Mineralization at Kara, Northwestern Tasmania: Evidence from Mineral Chemistry and Stable Isotopes. *Econ. Geol.* **2000**, *95*, 1215–1230. [CrossRef]

70. So, C.-S.; Rye, D.M.; Shelton, K.L. Carbon, hydrogen, oxygen, and sulfur isotope and fluid inclusion study of the Weolag tungsten-molybdenum deposit, Republic of Korea; fluid histories of metamorphic and ore-forming events. *Econ. Geol.* **1983**, *78*, 1551–1573. [CrossRef]

71. Nabelek, P.I. Stable isotope monitors. In *Contact Metamorphism*; Kerrick, D.M., Ed.; Reviews in Mineralogy: Chantilly, VA, USA, 1991; Volume 26, pp. 395–435.

72. Friedman, I.; O'Neil, J.R. Compilation of stable isotope fractionation factors of geochemical interest. In *Data of Geochemistry*; Fleischer, M., Ed.; United States Government Printing Office: Washington, DC, USA, 1977.

73. Hall, D.L.; Cohen, L.H.; Schiffman, P. Hydrothermal alteration associated with Iron Hat skarn deposit, San Bernardino County, California. *Econ. Geol.* **1988**, *83*, 568–587. [CrossRef]

74. Zürcher, L.; Ruiz, J.; Barton, M.D. Paragenesis, elemental distribution, and stable isotopes at the Peña Colorada iron skarn, Colima, Mexico. *Econ. Geol.* **2001**, *96*, 535–557. [CrossRef]

75. Taylor, H.P. Comparison of hydrothermal systems in layered gabbros and granites and the origin of low ^{18}O magmas. *Geochem. Soc. Spec. Publ.* **1987**, *1*, 337–357.

76. Ashley, P.M.; Andrew, A.S. The Mt Ninderry acid sulphate alteration zone and its relation to epithermal mineralization in the North Arm Volcanics, southeast Queensland. *Aust. J. Earth Sci.* **1992**, *39*, 79–98. [CrossRef]

77. Sun, S.S.; Eadington, P.J. Oxygen isotope evidence for the mixing of magmatic and meteoric waters during tin mineralization in the Mole Granite, New South Wales, Australia. *Econ. Geol.* **1987**, *82*, 45–52. [CrossRef]

78. Taylor, H.P. Oxygen and hydrogen isotope studies of plutonic granite rocks. *Earth Planet. Sci. Lett.* **1974**, *38*, 177–210. [CrossRef]

79. Taylor, B.E.; O'Neil, J.R. Stable isotope studies of metasomatic Ca-Fe-Al-Si skarns and associated metamorphic and igneous rocks, Osgood Mountains, Nevada. *Contrib. Mineral. Petrol.* **1977**, *63*, 1–49. [CrossRef]

80. Baranov, E.N.; Grinenko, L.N.; Pavlov, G.P. Pyrite sulfur isotope compositions in Ural skarn-magnetite deposits. *Geochem. Int.* **1986**, *23*, 81–90.

81. Cumming, G.L.; Richards, J.R. Ore lead isotope ratios in a continuously changing earth. *Earth Planet. Sci. Lett.* **1975**, *28*, 155–171. [CrossRef]

82. Meinert, L.D. Compositional variation of igneous rocks associated with skarn deposits—Chemical evidence for a genetic connection between petrogenesis and mineralization. *Mineral. Assoc. Can. Short Course* **1995**, *23*, 401–418.

83. Newberry, R.J. The formation of sub-calcic garnet in scheelite-bearing skarns. *Can. Mineral.* **1983**, *21*, 529–544.

84. Frietsch, R.; Tuisku, P.; Martinsson, O.; Perdahl, J.-A. Early proterozoic Cu, Au, and Fe ore deposits associated with regional NaCl metasomatism in northern Fennoscandia. *Ore Geol. Rev.* **1998**, *12*, 1–34. [CrossRef]

85. Steven, N.M.; Moore, J.M. Pan-African tungsten skarn mineralization at the Otjua Prospect, central Namibia. *Econ. Geol.* **1994**, *89*, 1431–1453. [CrossRef]

86. Zhao, Y.; Lin, W.; Bi, C.; Li, D.; Jiang, C. *Skarn Deposits of China*; Chinese Academy Geological Sciences: Beijing, China, 1994.

87. Kodera, P.; Rankin, A.H.; Lexa, J. Evolution of fluids responsible for iron skarn mineralization: An example from the Vyhne-Klokoc deposit, Western Carpathians, Slovakia. *Mineral. Petrol.* **1998**, *64*, 119–147. [CrossRef]

88. Ashley, P.M.; Billington, W.G.; Graham, R.L.; Neale, R.C. Geology of the Coalstoun porphyry copper prospect, southeast Queensland, Australia. *Econ. Geol.* **1978**, *73*, 945–965. [CrossRef]

89. Lee, C.H.; Lee, H.K.; Kim, S.J. Geochemistry and mineralization age of magnesian skarn-type iron deposits of the Janggun mine, Republic of Korea. *Miner. Depos.* **1998**, *33*, 379–390. [CrossRef]

90. Meinert, L.D. Skarn, manto, and breccia pipe formation in sedimentary rocks of the Cananea mining district, Sonora, Mexico. *Econ. Geol.* **1982**, *77*, 919–949. [CrossRef]

91. Mueller, A.G. The Savage Lode magnesian skarn in the Marvel Loch gold-silver mine, Southern Cross greenstone belt, Western Australia, Part 1; Structural setting, petrography, and geochemistry. *Can. J. Earth Sci.* **1991**, *28*, 659–685. [CrossRef]